Investigation of Gas-Surface Dynamics Using an Ar Atomic Beam and Functionalized Self-Assembled Monolayers

Shelby F. Shuler

Thesis submitted to the Faculty of the Virginia Polytechnic Institute and State University
in partial fulfillment of the requirements for the degree of

Master of Science
in
Chemistry

Dr. John R. Morris, Chair

Dr. Brian M. Tissue

Dr. Daniel Crawford

April 23,2002
Blacksburg, Virginia

Keywords: self-assembled monolayers (SAMs), molecular beam, ultrahigh vacuum

Investigation of Gas-Surface Dynamics Using an Ar Atomic Beam and Functionalized Self-Assembled Monolayers

Shelby F. Shuler

(ABSTRACT)

Interactions of gas-phase molecules with surfaces are important in many ordinary events, such as ozone depletion, corrosion of metals, and heterogeneous catalysis. These processes are controlled by the bonding, diffusion, and reactivity of the impinging gas species. Our research employs molecular beam techniques and well-characterized surfaces to study these processes.

The goal of this study is to better understand how the physical and chemical nature of the surface interface influences energy transfer dynamics in gas-surface collisions. An atomic beam is used to probe the energy transfer dynamics in collisions of Argon with model surfaces of functionalized self-assembled monolayers (SAMs) [$HS(CH_2)_{11}CH_3$ & $HS(CH_2)_{11}OH$] on gold. The beam is directed towards the surface at an incident angle of 30° and the scattered Ar atoms are detected at the specular angle of 30°. Time-of-flight scans measure the velocity distributions of atoms leaving the surface, which correlate with the energy transfer dynamics of the impinging gas atoms.

Gas-surface energy transfer experiments are accomplished by directing an 80 kJ/mol Ar atomic beam at a clean Au(111) surface and surfaces composed of OH-terminated or CH_3-terminated SAMs on Au(111). The fractional energy transferred to the bare gold surface is 69 %, while it is greater than 77 % for the monolayer-covered surfaces. The extent of thermalization on the surface during the collision is significantly greater for the CH_3-terminated surface than for the OH-terminated surface. Since the two monolayers are similar in structure, packing density, and mass, the differences in scattering dynamics are likely due to a combination of factors that may include differences in the available energy modes between the two terminal groups and the hydrogen-bonding nature of the OH-terminated SAM.

Acknowledgments

First and foremost, I would like to thank God for allowing me to study, understand, and perform to the best of my ability.

Dr. John R. Morris for his support and advice.

The Morris' group: Gwen Davis, Scott Day, James Lohr, and Melinda Ferguson.

I would like to thank my committee members, Dr. Tissue and Dr. Crawford for serving and critiquing my thesis.

A special thanks goes to Dr. Michael L. Myrick and Paula E. Colavita from The University of South Carolina for their contributions of the STM images.

I would like to thank Dr. Dessey and his wife for their kindness and encouragements.

A special thanks goes to MAOP for funding me during the Spring and Summer 2001 sessions.

Last, but not least, I would like to thank my family for their love and support.

TABLE OF CONTENTS

LIST OF FIGURES

LIST OF TABLES

LIST OF EQUATIONS

Chapter 1

Introduction and Motivation

1.1 Gas-Surface Interface

Interactions of gas-phase molecules with surfaces are important in many ordinary events, such as ozone depletion, corrosion of metals, reactions at pulmonary interfaces, and heterogeneous catalysis. Many of these processes depend primarily on the bonding, diffusion, and reactivity of the impinging gas species. For example, Nathanson *et al.* have studied and established numerous outcomes pertaining to different gas-phase molecules interacting with an H_2SO_4 liquid interface.[1-3] Their findings suggest that HCl and HBr desorb faster than they dissociate; thus, hindering the formation of Cl^- and Br^- in increasingly acidic aerosols. Studying the dynamics of collisions and reactions on this acidic surface has led to important information on the chemistry in the stratosphere and ozone destruction. Their contributions and others[4,5] have embarked on a new outlook for studying surface chemistry. Despite these efforts, there still exist many unanswered questions regarding gas-surface reactions including: Do reactions occur on the surface or beneath the immediate surface interface? What types of functional groups make a surface soft enough that it can absorb a gas molecule's impact energy, momentarily stopping the momentum of the molecule and allowing it to react with the surface? How do reactions occur in the absence of solvent? The overall goal of this study is to develop a better understanding of the general mechanisms of gas-surface bonding and reactions. The fundamental investigation that is presented in this paper involves the use of an Argon (Ar) atomic beam and functionalized self-assembled monolayers that terminate in OH, OD, and CH_3 to explore the initial gas-surface collision.

Previous experimental and theoretical studies have demonstrated that *n*-hexylthiolate self-assembled monolayer on Au(111) shields the underlying gold substrate

from high energy collisions by serving as a heat bath to efficiently dissipate the kinetic energy of the impinging atoms or molecules.[6,7] In addition, the mass of the molecules used to create a monolayer has been shown to have a marked affect on the gas-surface energy transfer dynamics.[8,9] The results of our work will extend these studies and set a foundation for understanding how the chemical nature of the interface influences energy transfer dynamics in gas-surface collisions. Future experiments will explore these dynamics in more detail by exposing reactant gases (e.g. HCl, HBr, HNO_3, or NH_3) to these model surfaces with different chain terminal groups (e.g. OH, NH_2, COOH, or $CONH_2$). Through this systematic approach, reaction modes such as hydrogen bonding, proton exchange, and acid-base bonding will be examined.

1.2 Atomic and Molecular Beam Techniques

In the mid-1970s, the first instrument capable of energy transfer measurements at well-characterized surfaces under an ultrahigh vacuum environment was developed at the University of Chicago.[10] The Chicago group used a Xe beam directed at a Pt(111) surface to study velocity and angular distributions for Xe scattering. Atomic/molecular beams are useful methods because they can perform on the level of producing such well-defined energies and geometries; and they provide vital information about the incident atom or molecule that is helpful in understanding the surface interaction or dynamics. In order to maintain the well-defined energies, the beam must be produced in a vacuum and kept under a vacuum regime until it reaches the surface. Further details in Chapter 2 will describe the apparatus and vacuum requirements necessary to form intense beams.

The mechanism behind the beam technique is quite straightforward. An atomic or molecular beam is projected at the surface with a desired incident angle (θ_i) and incident energy (E_i). The scattered species are detected at the specular angle (the angle at which the angle of reflection equals the angle of incidence) with a quadrupole mass spectrometer. Angular distributions of the scattered species can be obtained if the mass spectrometer is rotatable. The arrival times of the scattered species are used to determine

the velocity distributions, which correlate with the energy transfer dynamics of the impinging gas atoms or molecules.

1.3 Scattering Dynamics: Inelastic, Elastic, and Thermal-Desorption

In gas-surface experiments, not every gas species scattering from a surface will experience the same type of collision. Some atoms or molecules might endure longer residence times on the surface than others, especially if some species undergo multiple collisions or react with the surface in some manner. The non-reactive scattering pathways can be categorized into three distinct channels: direct inelastic scattering (IS), elastic scattering, and thermal-desorption (TD). There is a fourth channel that is considered only in reactive scattering cases and it is worth mentioning. This particular channel is known as thermal-reaction-desorption and this has been described in the work of gas-liquid encounters.[11,12]

The most common channel that is recognized in non-reactive scattering is the inelastic scattering channel (see Figure 1.1). This channel can be defined as the impinging gas atoms or molecules directly reflecting and exchanging both parallel and normal motion with the surface in an inelastic single collision.[10] During this single collision event, the gas species can either gain or lose energy from the surface and this is highly contingent on their incident energy. Furthermore, the inelastically scattered gas species retain some information regarding their original incident trajectories.

The elastic scattering channel is the counterpart of inelastic scattering in that the impinging gas species merely collide with the surface without transferring any energy and this phenomenon is normally applied to light atoms (e.g. He) or molecules (e.g. H_2). In this study, the elastic channel is negligible in surface scattering since a heavier Ar atom is being employed.

The third and final channel that is seen in typical gas-surface scattering experiments is thermal-desorption. Thermal-desorption occurs when the gas species thermally equilibrate with the surface before desorbing; thus, losing all of their initial

incident energy and trajectory information. This desorption component results in a Maxwell-Boltzmann velocity distribution, characterized by the surface temperature.

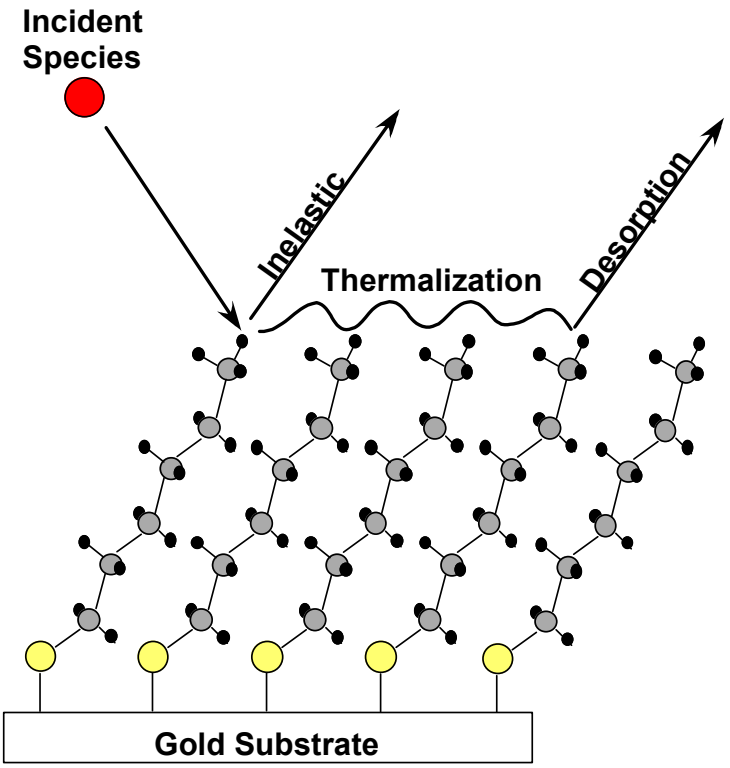

Figure 1.1. Possible pathways for an incident atom or molecule colliding into functionalized self-assembled monolayers. The yellow circles represent thiol atoms, the gray circles represent carbon atoms, and the black circles represent hydrogen atoms. Incident species undergoing thermalization usually experience ps residence times.[6]

1.4 Surface Interface: Self-Assembled Monolayers on Gold

Self-assembled monolayers are organic molecular assemblies that present unparalleled opportunities to increase fundamental comprehension of interfacial phenomena, self-organization, and structure-property relationships.[13] These monolayers make excellent model surfaces since they provide the ability to control surface order,

structure, and functionality (see Chapter 3). In addition, very little is known concerning the comparisons and differences between energy transfer in collisions of atoms or molecules with these organic molecular assemblies.

The outcome of a gas-surface collision depends on the mass, size, incident energy, and incident angle; however, the surface also plays a vital role. Most surfaces act as a second reactant in conjunction with the gases. The experiments in this study will use simple alkylthiol monolayers in a way that the functional end groups represent the surface since the monolayers are closely packed on the gold substrate, and the long-chain hydrocarbons are used as the framework for the molecular assemblies. The thiol groups are chemisorbed to the Au(111) substrates and serve as an anchor for the monolayers. X-ray photoelectron spectroscopy and scanning tunneling microscopy will be used to characterize the surfaces in a quantitative and qualitative manner, respectively.

Chapter 2

Experimental Approach and Instrumentations

2.1 Molecular Beams

The most vital component in gas-surface scattering studies is the production of stable, well-collimated molecular beams. Producing molecular beams requires several components: gas of interest, a nozzle, a skimmer, chopper wheel, and vacuum chambers. Each component is important in the production of the beam and must routinely be checked for optimal use. In order to provide adequate information about energy transfer dynamics at the surface, a molecular beam is projected at the surface and the scattered species are detected as a function of mass and arrival time. In an ideal experiment, expanding the gas through a nozzle produces the beam. The nozzle aperture is typically 25-30 μm in diameter, and the beam undergoes adiabatic cooling during expansion.[14] Most of the translational energy is focused into the direction of the beam. As the beam departs from the nozzle, it will pass through the skimmer. This cone-like shaped skimmer is precisely aligned with the nozzle and both are mounted in the source chamber (see Figure 2.1). The purpose of the skimmer is to reflect the shock wave formed upon the high pressure expansion of the gas into the vacuum before the wave collapses on itself; thus, deflecting the beam's trajectory and compromising its monoenergicity.[15] The beam then enters two differential pumping stages that are usually produced by diffusion and turbo molecular pumps. Creating molecular beams under these conditions will produce a flux (10^{11}-10^{15} molecules/cm^2 s) from the beam on the surface that is larger than the flux from the background gas in the main chamber. Finally, the beam is pulsed by passing through a rotating chopper wheel before entering a small orifice that leads to the main chamber. The chopper wheel is extremely important for two reasons: (a) it

modulates the beam intensity into the main chamber; and (b) the slots provide an opening for the trigger pulse that represents the start of a beam pulse.

This overview should allow the reader to understand the fundamental aspects of producing molecular beams and the significant influences they will have on studying surface chemistry. The experiments and techniques that will be described in the following sections will give a better insight on forming molecular beams.

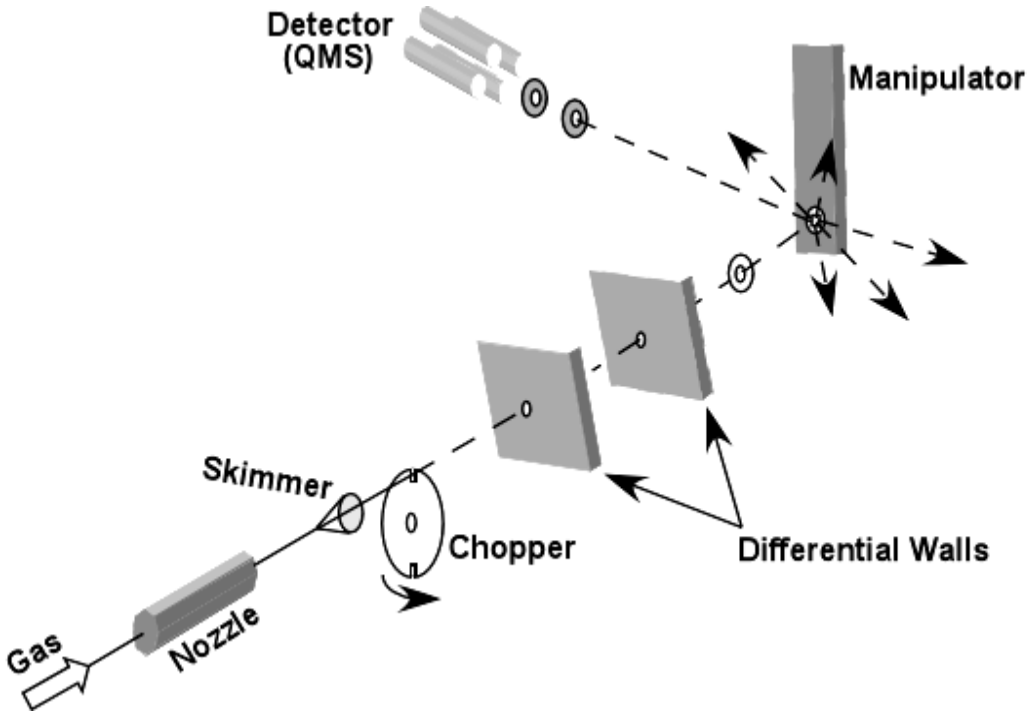

Figure 2.1. Shows a schematic representation of the molecular beam scattering apparatus.

2.1.1 Beam Source and Technical Description

The experiments that are performed involved the use of Ar gases. These particular gas cylinders are purchased from Matheson Inc. Each cylinder also contains a carrier gas along with the gas of interest. The purpose of the carrier gas is to increase the kinetic energy of the impinging gas atoms. The gas cylinders for Ar are mixtures of 2 % Ar/98

% H_2 for the high-energy beam, 5 % Ar/95 % He for the low energy beam, and 100 % ultra-high purity Ar is also used. Stainless steel regulators are attached to each Ar cylinder for maintaining purity of the gas before entering the source chamber. Teflon® tubing is connected to the regulators via swagelok. The other end of the tubing is attached to a constructed stainless "T" valve swagelok. A mechanical roughing pump is used to eliminate any undesired gas in the beam source line before opening the valve to the source chamber.

2.1.2 Source Chamber

As mentioned in the overview section, the source chamber is where the molecular beam originates. The nozzle orifice has a diameter of 50 μm and is commercially available from Parker Instrumentation along with the nozzle controller. The controller, which opens and closes the nozzle, is set to a continuous opening time. After opening the nozzle, a 6 V power supply is used to maintain the opening because the nozzle controller output voltage of 24 V is too high. This high output can cause excessive heating near the nozzle orifice and it can affect the beam. When the beam passes through the nozzle, a small skimmer accurately aligned and mounted with the nozzle extracts the centerline beam. The skimmer is fabricated from Ni and the aperture is 0.4 mm in diameter. This particular skimmer is commercially available from Beam Dynamics Inc.

Since the experiments are time-resolved, a slotted chopper wheel manufactured by the department machine shop is installed in the source chamber. This Al wheel has a 5″ diameter; a thickness of 0.64 mm and the two slots are 8.9 mm (length) × 1.6 mm (width). The slots are situated in an opposing fashion and an in-lab built motor controller controls the chopper wheel. The wheel rotates counter-clock wise at 300 Hz for all experiments. A light-emitting diode (LED) and photodiode device that is located slightly above the wheel provides the signal. This device has a 6 V power supply and as the slots passes between the LED and photodiode, the trigger signal from the photodiode is transformed into ~24 μs width transistor-transistor logic (TTL) pulses. A Tektronix TDS

220 Oscilloscope is used to monitor these pulses as they are relayed through a coaxial cable to the multichannel scaler.

The vacuum in the source chamber is quite unique compared to the remaining vacuum system. The source chamber for our system is equipped with a VHS-10 Diffusion Pump, a Diffstak® Mk2 Diffusion Pump, and one turbomolecular pump (TMP). The maximum pumping speeds are 5000 ls^{-1}, 1500 ls^{-1}, and 250 ls^{-1}, respectively. The VHS-10 Diffusion Pump (Varian Vacuum Technologies) in this chamber pumps out an enormous amount of gas from the source chamber. Only a small fraction of gas (centerline beam) passes through the skimmer. The pressure in the source chamber is usually maintained around 2×10^{-4} mbar and this pressure is adjusted accordingly from the cylinder regulator. The Diffstak Diffusion Pump (BOC Edwards 160/700 model) is located near the main chamber along with the turbomolecular pump (Pfeiffer TMU261P). These two pumps create two differential pumping stages and the pressure is on the order of 1×10^{-6} mbar. The stages are separated by 7.9 mm thick walls and contained in each wall is a collimating aperture. The first aperture is 1.5 mm in diameter and the second aperture is 2.7 mm. The beam passes through the apertures into the differential pumping stages and the beam produces a 1-cm spot size on the surface sample located in the main chamber, 35 cm from the nozzle.

2.2 Ultrahigh Vacuum System

Studying surface chemistry in an ultrahigh vacuum (UHV) environment, usually $<1 \times 10^{-9}$ mbar, is very crucial. In order to be successful, the surface must remain clean and well characterized during the experiment. The UHV system only involves the main and detector chambers. The following sections will discuss and describe the UHV system that is used along with the necessary components to perform molecular beam scattering experiments in this system.

2.2.1 Main Chamber

The main chamber is the core of the molecular beam scattering apparatus (see Figure 2.2). This cylindrical shaped chamber has an inner diameter (i.d.) of 12″ and it is 25.3″ in length. The chamber is fitted with numerous Conflat® flanges and viewing windows. These flanges have conical knife-edges and sealing is accomplished by incorporating a Cu gasket between the chamber and flange. The source chamber is connected to the main chamber with a 6″ outer diameter (o.d.) flange and an 8″ o.d. flange is used for the detector chamber. The main chamber also contains several gate valves and a manipulator, which is coupled to the chamber apex.

The manipulator (McAllister MA2012 model) is used to allow the surface to be positioned in any manner without compromising the UHV environment. This particular device enables the surfaces to be translated in an x-y-z direction and it also provides three rotational degrees of freedom. The z-translation is controlled by a stepper-motor and the x,y-translations are adjusted by manual micrometers. The surfaces are mounted to the end of the manipulator inside the chamber. This Cu block end is composed of a heater and a liquid N_2 reservoir. In addition, electrical and cryogenic feedthroughs are implemented for the heater and liquid N_2 reservoir. The heater is used only for temperature-programmed desorption (TPD) experiments. A thermocouple wire that is spot welded to the surface sample holder monitored the temperatures of the surface. This stainless steel holder uses tabs to clamp down the surfaces and the holder is attached to the Cu block via load lock system.

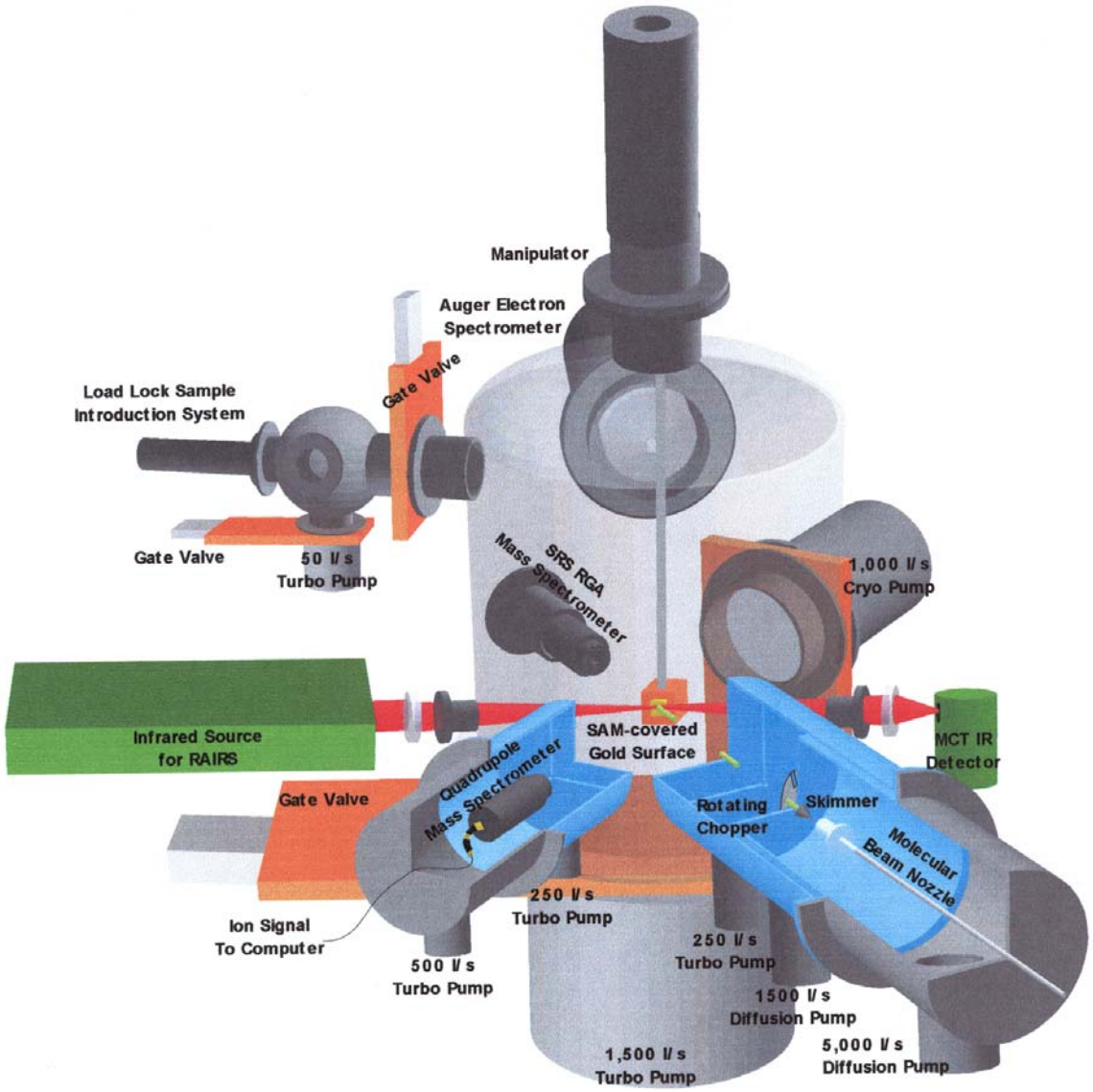

Figure 2.2. Shows ultrahigh vacuum molecular beam scattering and surface analysis apparatus for investigating the mechanisms of gas-surface reactions.

The load lock system (MDC Vacuum Products Corp.) is an efficient method to transfer the sample to the main chamber. This system has a fork-like shape receptacle-rotating arm and a small TMP (Pfeiffer TMU071P) is connected to the load lock chamber. After venting the chamber with ultrahigh pure N_2, the desired sample is secured into the receptacle arm. The load lock chamber is then evacuated by the use of the small TMP, which has a maximum pumping speed of 50 ls^{-1}. The pressure in the load lock chamber is usually on the order of 2.0×10^{-6} mbar before opening the manual load lock gate valve to the main chamber. The manipulator parameters for installing and retrieving samples are set to 8.5 μm (x-translation), 5.75 μm (y-translation), 0.75″ (z-translation), and the angle is set at 150°. After opening the gate valve, the arm is pushed in immediately until the sample holder contacts the Cu block. The arm is rotated until the holder is fastened into place. After securing the holder, the arm is retracted and the load lock gate valve is closed.

In order to perform molecular beam scattering experiments, the surfaces must be properly aligned with the source chamber. Surface alignment plays an important role in obtaining the desired incident angle of the molecular beam and detecting the beam at the specular angle. To align the surface, the surface normal is aligned directly to the detector chamber and the manipulator micrometers are set to 8.5 μm (x-translation) and 7.55 μm (y-translation). The manipulator is lowered to 11.26″ (z-translation) and the surface is rotated to an angle of 187.9°. A HeNe laser shining through the rear-viewing window of the detector chamber onto the surface is used to check the alignment. After the surface is aligned to the detector chamber, it is rotated to an angle of 218°. At this point, the light shining through the detector chamber onto the surface is deflected in the direction of the aperture to the source chamber. The incident angle of the beam is 30° from the surface normal (see Figure 2.3).

The incident angle and energy of a beam are extremely important parameters in determining the outcome of the gas collision. Furthermore, the beam must be well defined in order to study the fractional energy transferred to the surface. The beam energies are controlled by the nozzle temperature, backing pressure, and mass ratio of the

carrier gas to the gas of interest. Several different incident energies are utilized for the Ar scattering experiments: 2 % Ar/98 % H_2 (E_i = 80 kJ/mol), 5 % Ar/95 % He (E_i = 40 kJ/mol), and 100 % Ar (E_i = 6 kJ/mol). These energies are measured with the assistance of a SRS RGA (Stanford Research Systems Residual Gas Analyzer) Mass Spectrometer that is coupled to the main chamber. This particular instrument is positioned directly across from the source chamber (see Figure 2.2). The manipulator is raised approximately 2-4″ above the normal scattering position; thus, allowing the beam to directly enter the mass spectrometer. The incident energies are determined experimentally using the peak arrival time of the beam and the distance from the chopper wheel to the ionizer. The translational energy of the beam is conserved due to the absence of collisions in the UHV environment.

The UHV in the main chamber is produced via two pumps, a Cryo-Plex 8 UHV Cryopump (Austin Scientific Company Inc.) and a large TMP (Pfeiffer TMU1601P), with maximum pumping speeds of 1000 ls^{-1} and 1500 ls^{-1}, respectively. The pressure in the main chamber is usually maintained around 9×10^{-10} mbar. The main TMP is attached to the base of the main chamber and the cryopump is situated 10″ away from the normal scattering position of the surface. The cryopump is coupled to the main chamber via a gate valve (10″ o.d. flange). This pump is equipped with a He compressor that is used to cool the cold head and it is particularly good for removing any H_2O vapors inside the chamber.

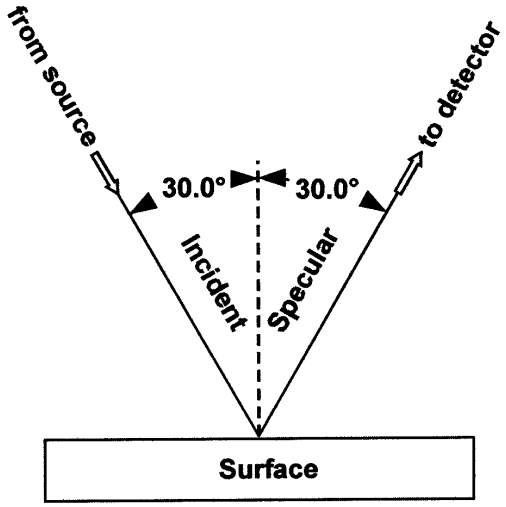

Figure 2.3. Illustrates the experimental geometry used for scattering molecular beam from surface. The dotted line represents the surface normal.

2.2.2 Detector Chamber

One of the main objectives of our work involves monitoring the energy transfer dynamics and thermal-accommodation of impinging atoms or molecules. Any gas-phase species that undergo inelastic scattering or thermal-desorption at the specular angle will be detected. The detector chamber consists of a quadrupole mass spectrometer (QMS), purchased from ABB Extrel (MEXM1000 model), and two turbomolecular pumps (TMPs) that are used to create a doubly differential pumping environment. Under these conditions, the residual background gas from the outgassing of the ionizer is reduced while maintaining the signal intensity. The orifice to the first differential stage is 4.3 mm in diameter and this stage is pumped on with a Pfeiffer TMU261P (speed of 210 ls^{-1}). The second differential stage contains a 4.7 mm orifice and the QMS is seated in this stage. A Pfeiffer TMU521P (speed of 500 ls^{-1}) is used to produce the vacuum in the second stage. The pressure in the detector chamber usually remained on the order of 9.0 $\times 10^{-10}$ mbar. The detector chamber is located 60° away from the source chamber and the

mean free path from the surface to the ionizer is ~14″. The QMS is equipped with a pulse counting electron multiplier/preamplifier, RF filter, electron impact axial ionizer (Tungsten filaments), and a mass resolution over a 2-1000 amu range. The electron multiplier is set to 2000 V and the dynode is set to 4000 V for all experiments conducted.

2.2.3 Interlock System

Performing experiments in vacuum can be expensive, but practical if the vacuum apparatus is well managed and monitored. The interlock system provides a way to protect the instruments from unauthorized pressure bursts and power losses. This system is developed from the LabView programming language and FieldPoint relay modules (National Instruments Inc.). The modules are installed inside the interlock box, which is connected to the computer interface. The box contains a series of switches on the front panel that are used to control the opening or closing of various gate valves and foreline valves. The switches have three mode settings: “on”, “computer”, and “off”. In the “computer” position, the interlock program is initiated to monitor any irregularities in pressures and this is accomplished with the support of the FieldPoint modules. If the pressure in any chamber increased above the desired set point pressure, the FieldPoint switch would open; thus, discontinuing the power to the TMPs and closing the gate valves.

The front panel of the interlock program allowed convenient access to operate the gate valves, TMPs, and foreline valves (see Figure 2.4). Chamber pressures are displayed in the yellow indicator boxes and the set point pressures are located beneath them. The “Vent for Sample” and “Evacuate” buttons are used for the load lock chamber. The graph-like picture on the main chamber plotted the main chamber pressure versus time and it depicts the pressure over a 24 hour time period.

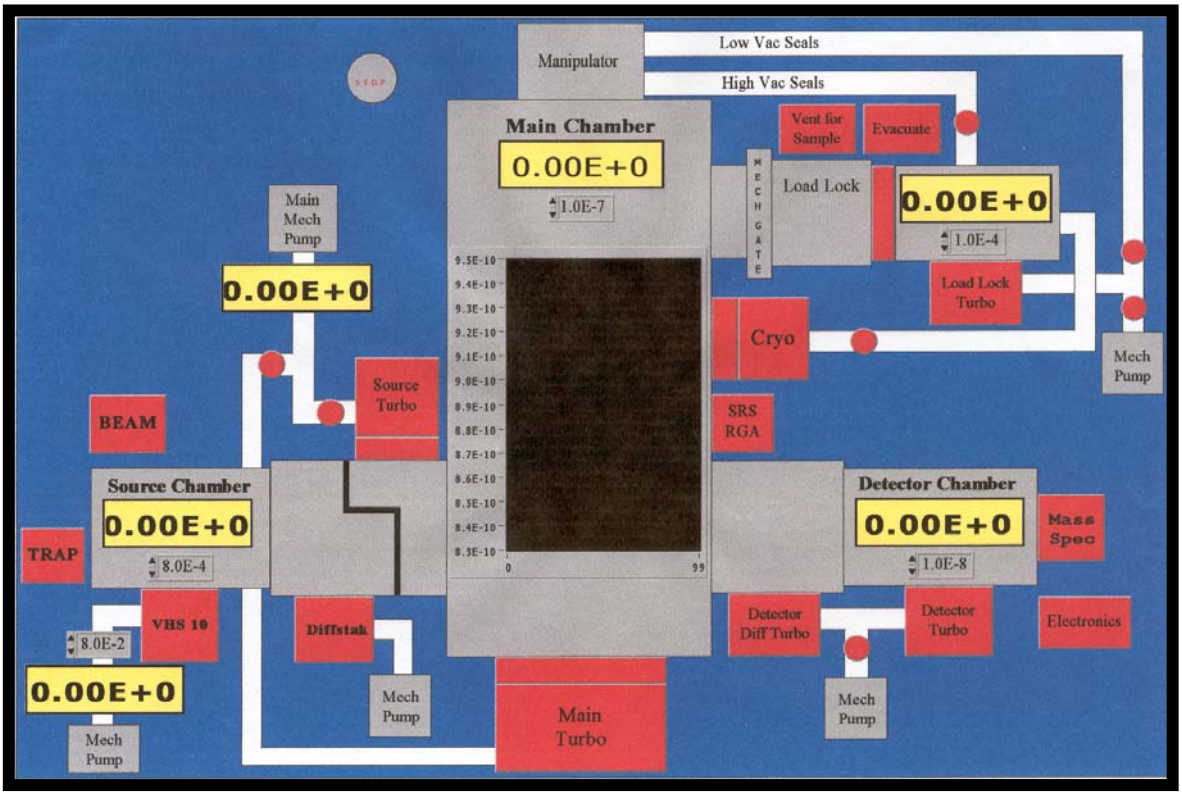

Figure 2.4. Shows the front panel of the interlock program.

2.3 Data Acquisition

The time-of-flight (TOF) data is obtained from the QMS by using a multichannel scaler (MCS). The TOF analysis is achieved through the synchronization of the trigger signal from the photodiode device (in source chamber) and the signal from the QMS. The distribution of atoms or molecules departing from the surface is measured as a function of mass and arrival time. The adjusted arrival time is established from the experimental timing, offset timing, and the QMS residence timing.

2.3.1 Multichannel Scaler

A MCS (Ortec®) is used to collect and record the TOF data. This scaler consists of a MCS-32 software and MCS-pci plug-in card. The card contains a dual-port memory that allows computer access to the spectral data, without interfering with data acquisition. The card parameters are dwell times ranging from 100 ns to 1300s, a memory length of 65,536 channels, and input counting rates up to 150 MHz. The MCS also offers versatile scan synchronization.

During an experiment, the transistor-transistor logic (TTL) pulses from the photodiode are relayed directly to the "Start Input" of the MCS-pci that initiates the scan. Simultaneously, the signal from the QMS is relayed through a F-100T Preamplifier-Discriminator (Advanced Research Instruments Corp.) to the MCS-pci.

The MCS-32 software provides the graphical display of TOF data. The horizontal coordinate corresponds to the selected dwell time (or bin width), which is set to 10 μs. The pass length is set to 198 channels and the number of scans is set to 100,000 for all experiments conducted. Three sets of spectral data are recorded for each surface and they are compared to each other in the MCS-32 buffer.

2.3.2 Time-of-Flight Analysis

The TOF scans measure the velocity distributions of atoms or molecules leaving the surface. The TOF has three pathways: (a) the gas-phase flight time from the chopper to the surface, (b) the residence time on the surface, (c) and the gas-phase flight time from the surface to the detector. Since the residence time on the surface is too small to measure (~ps or fs)[6], the residence time is negligible in determining the adjusted arrival time. This adjusted arrival time is defined by using this equation:

$$t(\text{arrival}) = t_{exp} + (\text{FBO}) - \alpha\sqrt{M} \qquad \textbf{(Equation 2.1)}$$

where t_{exp} is the gas phase flight time from the chopper to the detector, FBO (Front-Back Offset) is the offset timing from the chopper wheel (this number is negative due to the

counterclockwise spinning direction of the wheel), $\alpha\sqrt{M}$ is the time that the gas species spend in the QMS.

In order to measure the velocity distributions, t_{exp} is corrected by subtracting the gas-phase flight time from the chopper to the surface. This factor is measured experimental for each gas by using this relation: $t_{cs} = d_{cs}/v$, where t_{cs} is the beam flight time from the chopper to the surface, d_{cs} is the distance from the chopper to the surface, and v is the velocity of the beam. The flight times are 157 ms (Ar/H_2), 224 ms (Ar/He), and 564 ms (ultrahigh pure Ar). The FBO is approximately -917 μs.

2.3.3 Measuring Incident Energy

The beam incident energies are acquired from the use of the SRS RGA mass spectrometer and TOF technique. The energy for the ultrahigh pure argon is calculated at room temperature using this mathematical expression: $E = \sqrt{(5RT/M)}$, where R is the gas constant, T is the temperature (~298 K), and M is the mass of the gas. The peak arrival time for pure Ar (~900 μs) is obtained and this time is used to find the distance from the chopper to the ionizer of the SRS RGA MS. The computed distance is 49.17 cm and it is determined from this equation: $L = t_p\sqrt{(2E_i/M)}$, where t_p is the peak arrival time of pure Ar, E_i is the incident energy, and M is the mass of the gas. Using the TOF method, the peak arrival times for Ar/H_2 (high energy beam) and Ar/He (low energy beam) are ~250 μs and ~350 μs, respectively. These arrival times are used to find the incident energies from the $1/2mv^2$ relation, where a body of mass (m) is traveling at a speed (v).

2.4 Summary

The most vital component in gas-surface scattering studies is the production of stable, well-collimated molecular beams. Molecular beams are generated in the source chamber with the aid of a nozzle, skimmer, chopper wheel, and differential pumping stages. The beam interacts with the surface at an incident angle of 30° in the main chamber. An Ar atomic beam is used to probe the surface. The experiments that are performed required the use of an UHV system to prevent the surface from becoming

contaminated during a scattering experiment. A quadrupole mass spectrometer (QMS) detects the scattered atoms or molecules departing from the surface at the 30° specular angle. The time-of-flight (TOF) data is obtained from the QMS by using a multichannel scaler (MCS). The TOF analysis is achieved through the synchronization of the trigger signal from the photodiode device (in source chamber) and the signal from the QMS. The arrival time is used to determine the velocity distributions of scattered species, which correlate with the energy transfer dynamics of the impinging gas atoms or molecules.

Chapter 3

Surface Preparation and Characterization

3.1 Self-Assembled Monolayers

Self-assembled monolayers (SAMs) have been studied extensively over the past decade and their contributions to the chemistry community are significant.[16] These monolayers are ultra-thin organic molecular assemblies formed by the adsorption of an active surfactant on a solid substrate,[13] and they have three unique features: the terminal group, alkyl chain group, and the head-group (see Figure 3.1). The terminal group is an important part of the SAMs for our work because it is the first point of impact with gas-phase molecules or atoms. Another key factor that makes this group unique is the readiness of interfacial reactivity.[17] The second important feature of SAMs is the alkyl chain group. According to Nuzzo and Whitesides *et al.*, the chain length can have a major influence on the packing densities and ordering configuration on the surface.[18] SAMs are easily formed on the substrate via chemisorption of the head-group (e.g. sulfur). The chemisorption process is the phenomenon that enables the self-assembly to occur. Adsorption of SAMs can be accomplished by immersing the substrate into the appropriate diluted alkylthiol solutions.

The most commonly used SAMs are the *n*-alkanethiols on Au(111) substrates. These particular alkanethiols exhibit high thermal stability,[19] long-range order,[20] and homogeneity[21] on the surface. The properties that SAMs exhibit are beneficial to many applications, such as biomimetics, biosensing, and chemical sensing. Numerous surface analysis instruments have been used to verify these properties. The most conventional techniques for studying and characterizing SAMs on solid substrates are atomic force microscopy (AFM), X-ray photoelectron spectroscopy (XPS), scanning tunneling microscopy (STM), reflection-absorption infrared spectroscopy (RAIRS),

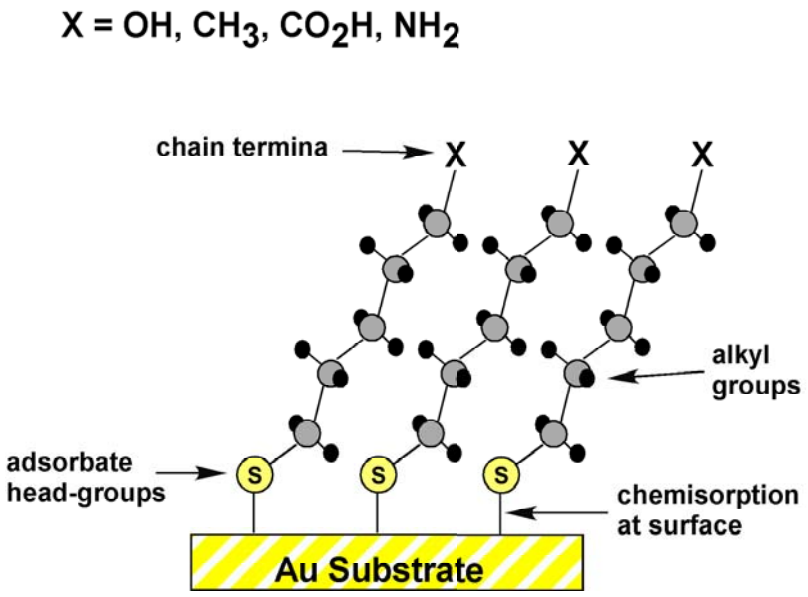

Figure 3.1. Shows a schematic side view of self-assembled monolayers adsorbed on gold substrate. Alkyl chains are organized in the trans (zigzag) conformation and the SAMs possess a 30° (±2°) tilt angle from the surface normal. Grey circles represent carbon atoms and black circles represent hydrogen atoms.

temperature-programmed desorption (TPD), and contact-angle measurements. Some of these methods are useful in that they are nondestructive and will allow the monolayer's integrity to remain intact.

SAMs make good model surfaces because they are well-ordered, stable, and most importantly, their terminal groups provide the opportunity to examine the energy transfer dynamics of gas-surface interactions on well-defined surfaces with different functionalities. For instance, the surface interface can be altered by the chemical nature of the terminal groups possibly influencing the energy transfer dynamics. The ultimate goal is to study the gas-surface adsorption and reactivity using *n*-alkanethiolates on Au(111) substrates.

3.2 Preparation of SAMs on Gold Substrates

SAMs are chemisorbed on Au substrates by immersing them in the proper alkylthiol solution and two types of substrates are used to demonstrate the effects of surface corrugation (in the context of molecular beam scattering from the surface), the glass posterior substrates (Evaporated Metal Films Corp.) and mica posterior substrates (Molecular Imaging). 11-Mercapto-1-undecanol [$HS(CH_2)_{11}OH$] and 1-dodecanethiol [$HS(CH_2)_{11}CH_3$] monolayers are purchased from Aldrich and used without further purification. The thiol solutions are prepared in absolute ethanol (Aapper Co.). XPS, RAIRS, STM, and TPD are used to characterize $HS(CH_2)_{11}OH$ (abbreviated OH-T, "T" stands for terminated) and $HS(CH_2)_{11}CH_3$ (abbreviated CH_3-T) on Au(111) substrates.

3.2.1 Evaporated Metal Film Substrates

Gold-coated glass surfaces provide the substrate for creating alkanethiol monolayers consisting of methyl- or hydroxyl-terminated end groups. These slides are created with 1000-2000 Å of Au, 50 Å of Cr, and SiO_2 posterior. The Cr is incorporated between the Au and SiO_2 to provide a means of adhering the Au to the SiO_2 support. The original dimensions of the glass slides are $1'' \times 1''$ and possess a thickness of 1 mm. The slides are modified ($0.5'' \times 0.5''$) in order to install them securely into the instruments. The modifications are performed in the department glass shop.

The gold slides are cleaned in a 3:7 mixture of 30 % H_2O_2/H_2SO_4 ("piranha" solution) at room temperature for approximately 1 hr, followed by extensive rinses in deionized water (Millipore Purification System, 18.2 MΩ) and dried under a stream of ultra-pure N_2. After cleansing, the slides are immediately deposited into a petri dish containing the dilute (~1 mM) thiol/ethanolic solution. The gold-coated glass slides remained in the solution for ~24 hr before removing. Prior to utilizing, the slides are rinsed with a copious amount of absolute ethanol and dried under a stream of ultra-pure N_2.

The OH-T SAMs are characterized in our group by RAIRS and XPS. The main purpose of this analysis is to investigate the chain conformation through examining the C-H stretching vibration modes. This information is used to confirm that the monolayers are adsorbed on the substrate in an organized fashion. Figure 3.2 shows the peaks of interest between 2800-3000 cm^{-1} in the RAIR spectrum of an OH-T SAM on Au(111). The broad absorption band emerging in the 3200-3600 cm^{-1} region is due to the lateral hydrogen bonding occurring between neighboring OH groups on the chain termina.[22,23] The $\nu_a(CH_2)$ and $\nu_s(CH_2)$ frequency bands are assigned to 2919 cm^{-1} and 2851 cm^{-1}, respectively. The highly intense $\nu_a(CH_2)$ peak suggests that the methylene groups are favorably oriented parallel to the surface normal.[22]

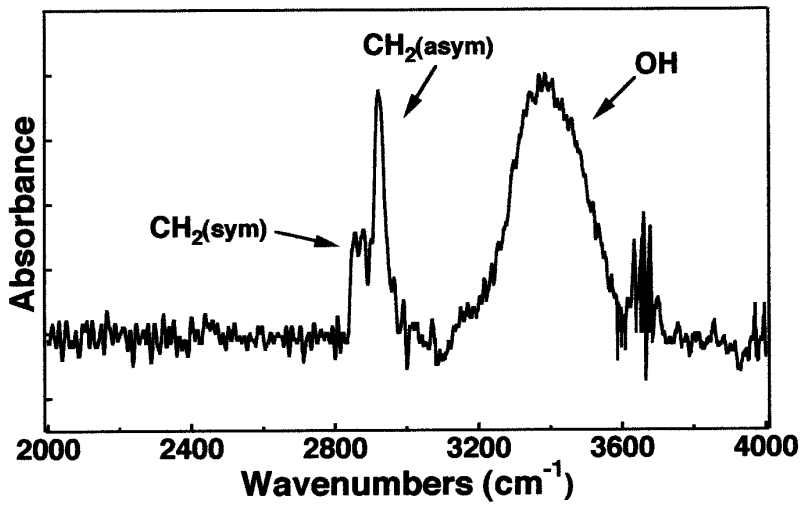

Figure 3.2. RAIR spectrum of $HS(CH_2)_{11}OH$ monolayers on Au(111) substrate (Evaporated Metal Film). The sample was measured on a Nicolat 710 RAIR Spectrometer with an HgCdTe detector.

The interpretation of this data verifies that the alkyl groups are in a trans-like conformation, which has been reported for several other SAMs on gold.[24,25]

3.2.2 Molecular Imaging Substrates

Well-ordered SAMs rely on a well-ordered, atomically flat Au substrate. The ideal surface is an atomically flat, smooth exterior with a (111) face structure and these substrates are commercially available from Molecular Imaging. The Au(111) substrates are fabricated by evaporating Au onto freshly cleaved heated mica substrates and atomically flat Au terraces (hundreds of nanometers) are produced after hydrogen flame annealing. The surfaces are usually 1.4 cm × 1.1 cm, with 1500 Å of Au covering a 1.0 cm × 1.1 cm area and they are used as received.

SAMs (OH-terminated & CH_3-terminated) on the Au/mica are prepared by submerging the substrates into the alkanethiol-containing ethanolic (~1 mM) solution for ~1 hr, while heating the solution to 60 °C. Prior to analysis, the substrates are flushed with copious amounts of absolute ethanol and dried under a stream of ultra-pure N_2 or Ar. Deuterium terminated (OD-T) SAMs are created from the OH-T monolayers using the same technique described above; thereafter, soaking the substrates in D_2O for ~1 hr. Glassware containing the thiol/ethanolic solution is always sonicated (Bransonic® 1510) in 95 % ethanol unless stated otherwise.

Samples that are generated on the Au/mica exhibit the same RAIR results as the samples on Au/Cr/SiO_2. This is valuable because the two substrates have different purposes. For example, the Au/mica surfaces are used mainly for STM, TPD, and molecular beam scattering. In contrast, the Au/Cr/SiO_2 surfaces are used for XPS and RAIRS. The mica-supported surfaces are ideal for STM because they are relatively flat and thin,[26] which is also important for heating in TPD. The glass-supported surfaces are ideal for XPS due to the simple fact that there is a rising edge to focus the X-ray source onto. Previous studies conducted in our group have shown that there are trivial discrepancies between the two types of substrates, despite the preparation procedures or method of characterization. Figure 3.3 illustrates the XPS surveys of the different surfaces and the surveys are consistent with the literature.[18] Figure 3.3(a) shows the OH-T SAM adsorbed on the glass posterior slide and Figure 3.3(b) represents the OH-T SAM adsorbed on the mica posterior slide. The XPS surveys are almost indistinguishable and

the Au peaks are labeled according to the orbital from which the emitted electrons originate (*the peaks that are not identified will be discussed in another section, see Figure 3.4*).

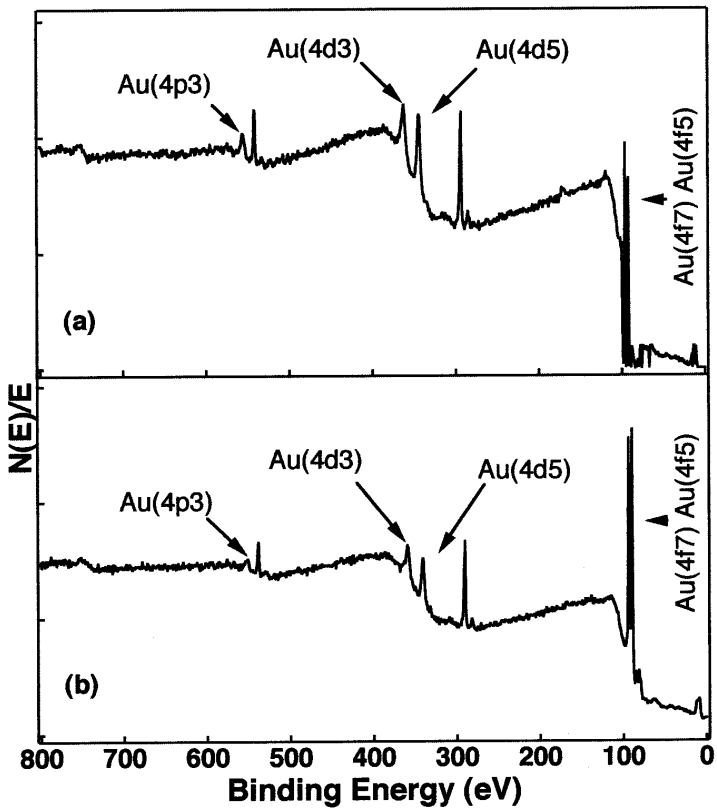

Figure 3.3. XPS surveys of $HS(CH_2)_{11}OH$ adsorbed on (a) Au(111)/glass posterior (Evaporated Metal Film); (b) Au(111)/mica posterior (Molecular Imaging). SAMs were prepared at 60 °C for ~1 h in solution. N(E)/E is the number of emitted electrons. (*Note: peaks that are nol labeled will be discussed in another section, see Figure 3.4*)

3.3 Mixed Self-Assembled Monolayers

The properties that SAMs exhibit alone are extraordinary and fascinating. The ability to control the surface properties is of great interest in the surface science field and this can be accomplished by using mixed monolayers. Mixed SAMs are usually comprised of two constituents. In the case of this study, a hydrophobic (CH_3-T) group and a hydrophilic (OH-T) group are used to create a binary mixture. Simply changing the composition of one co-adsorbed species in the bulk solution is found to have an impact on the surface composition.[21]

Mixed SAMs are prepared by making ~1 mM stock solutions (100 mL) of each alkanethiol. The 1-dodecanethiol (liquid) is made by weight, not by volume. The concentrations of the stock solutions must be as accurate as possible when producing mixed monolayers. The Au substrates are deposited for 1 h in the 1 mM solutions containing different ratios of OH-T and CH_3-T alkanethiols. The mixed solution is stirred for ~5 min before heating and upon transferring the sample to the load-lock chamber; the surface is rinsed extensively with absolute ethanol and dried under ultra-pure Ar.

3.4 X-ray Photoelectron Spectroscopy

The XPS measurements were performed on a Perkin Elmer 5400 X-ray photoelectron spectrometer with monochromatized Mg (Kα) radiation (1253.6 eV). The photoelectrons were analyzed at a takeoff angle of 15° with respect to the surface normal and the X-ray spot size was 1 mm × 3 mm. The managing base pressure was ~1.0×10^{-7} mbar and the total allotted acquisition time was 30 min for each sample. The powerstat was set to 14 kV and 300 W. The pass energy for the surveys was 44.75 eV and 17.9 eV for the multiplexes. For each multiplex conducted, the C(1s) peak was positioned to 285 eV by the means of adjusting the work function or anode energy. The surface compositions of mixed SAMs were calculated through the proportions of the O(1s) integrated peak areas for the mixed SAMs and the pure OH-T SAM. The O(1s) areas were normalized to the Au(4f7) that had a binding energy of 84.0 eV.

3.4.1 XPS Results and Discussion

X-ray photoelectron spectroscopy, also known as ESCA (Electron Spectroscopy for Chemical Analysis), is used for quantitative elemental analysis of mixed SAMs. In addition to the quantitative applications, XPS can be used as a qualitative tool via low resolution wide-scan survey. Figure 3.4 shows the surveys of the mixed monolayers $\{HS(CH_2)_{11}OH:HS(CH_2)_{11}CH_3\}$ on Au(111). The peaks of interest are the O(1s), C(1s), and S(2p) with approximate binding energies of 533 eV, 285 eV, and 162 eV, respectively.

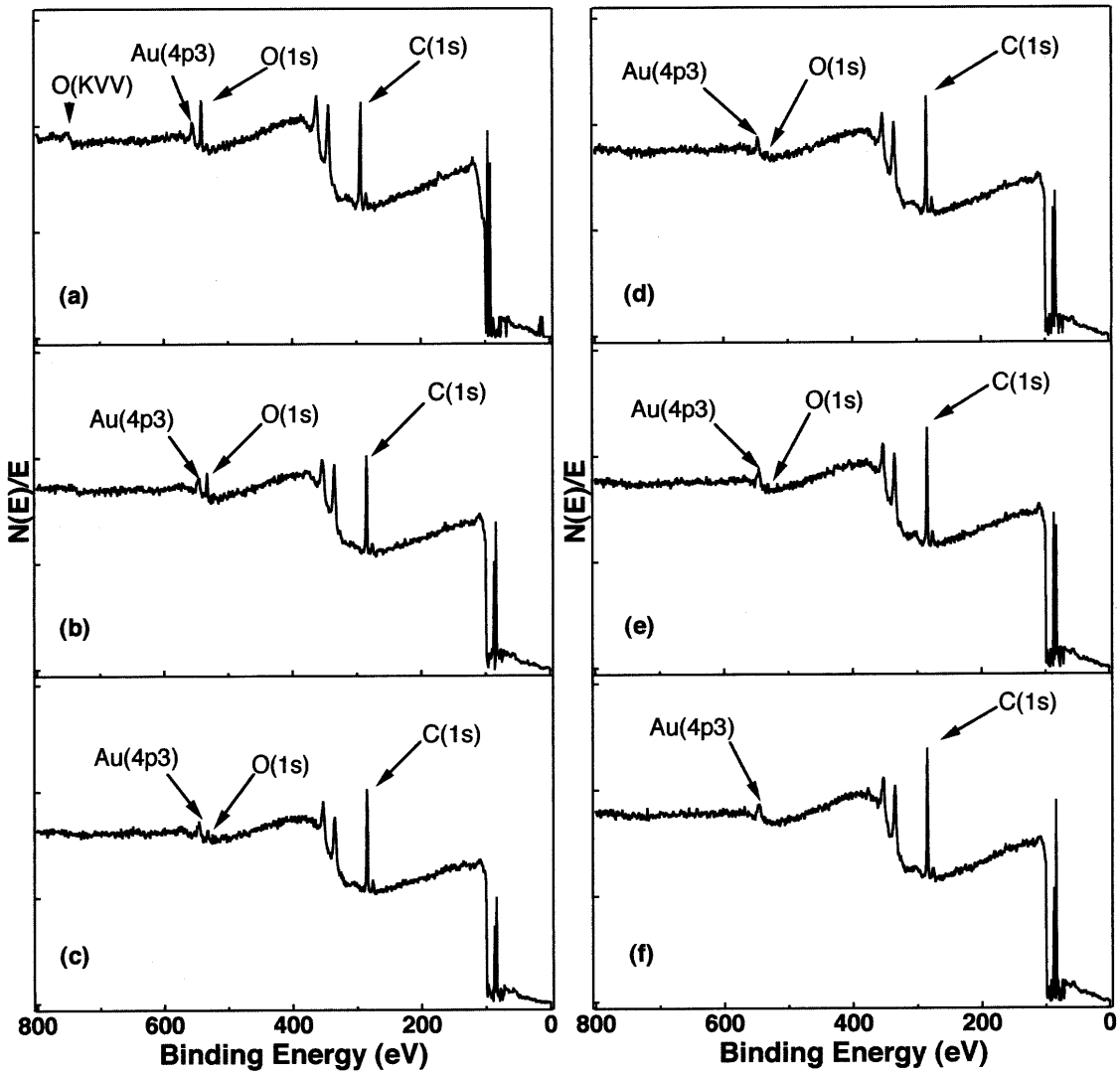

Figure 3.4. XPS surveys of mixed SAMs ([OH-T]:[CH_3-T]) on Au(111); (a) 100 % OH-T; (b) 0.8:0.2; (c) 0.6:0.4; (d) 0.4:0.6; (e) 0.2:0.8; (f) 100 % CH_3-T. Au and S peaks are not labeled for convenience.

The S(2p) peak (not labeled) is one of the most insightful peaks because it provides information on whether the monolayer forms gold-thiolate bonds,[27,28] and the measurements taken in this study are in agreement with the literature (see Figure 3.5). The second important observations are the C(1s) and the O(1s). The O(1s) intensity is

decreasing from (a) to (f) due to the decrease in mole fraction of OH-T SAM and corresponding increase of CH_3-T SAM in solution. Another indication that the monolayers are mixed on the surface is the decline in the emitted core electrons (~750 eV) from the oxygen *K*-shell.

Table 3.1. Summary of XPS surveys for mixed monolayers.

χ f(OH)$_{soln}$	χ f(OH)$_{surf}$	O(1s) areas (cts-eV/s)	Atomic Conc. O(1s)[a]
1	1	3950	8.29 %
0.8	0.731	2254	5.48 %
0.6	0.327	841	2.10 %
0.4	0.183	550	1.20 %
0.2	0.127	378	0.84 %
0	0	0	0 %

χ f(OH)$_{soln}$ is the mole fraction of OH-T SAM in solution and χ f(OH)$_{surf}$ is the mole fraction on the surface. [a]The empirical atomic concentration of oxygen on the surface.

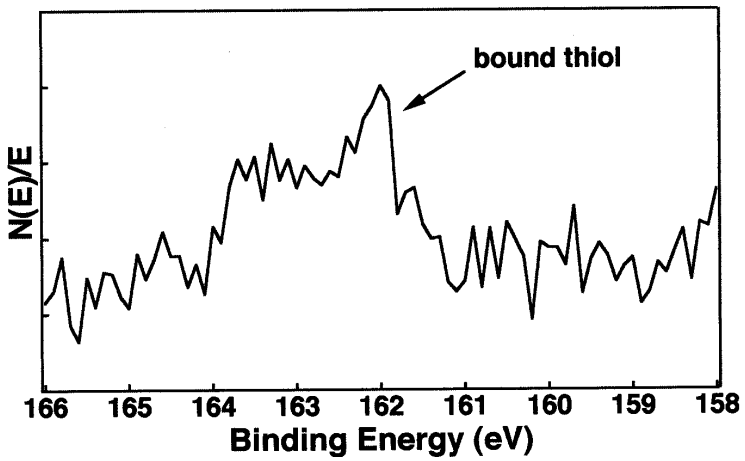

Figure 3.5. XPS spectrum of S(2p) for 100 % OH-T SAM adsorbed on Au(111). The same spectrum was observed for all mixed SAMs. The peak tailing may be due to the electrons that have lost their kinetic energy by inelastic collisions.

The data presents substantial evidence of mixed monolayers forming on the surface. The question that needs to be addressed is whether or not the surface composition is the same as the composition in bulk solution. As mentioned in section 3.3, the ability to manipulate the properties and attributes of a surface is of interest because SAMs can be used in a variety of applications. Initial studies[18,29,30] on this co-assembly network suggest that the chain length, solvent, and functional groups play an integral role in the surface composition. Figure 3.6 shows the mole fraction of OH groups on the surface as a function of mole fraction (OH) in solution. In a 50/50 mixture, the surface is only composed of ~30 % OH groups. Whitesides *et al*. have observed similar trends for the co-adsorption of $[S(CH_2)_{10}CH_3]_2$ and $[S(CH_2)_{10}CH_2OH]_2$ from ethanol.[21]

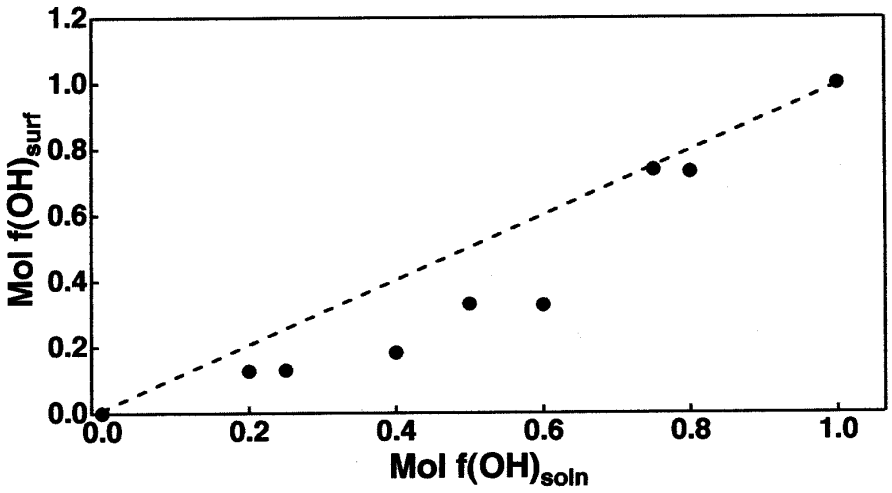

Figure 3.6. Illustrates the mole fraction of OH assembly on the surface relative to the mole fraction of OH in bulk solution from mixed monolayers ([OH-T]:[CH_3-T]). XPS integrated areas for O(1s) were normalized to the Au(4f7) of the pure OH-T SAM. The line represents the ideal 1:1 homogeneity slope.

The surface composition is characterized by the preferential adsorption of CH_3-T molecules and this behavior may be attributed to the hydrogen bonding effects of the OH-

T SAM.[21,31] It is also worth noting that the solvent has a major bearing on preferential adsorption and Whitesides *et al*. have demonstrated solvent effects by using an iso-octane solvent. In this study, the OH-T SAM was highly favored on gold; in contrast, ethanol solvent was found to create a highly favored CH_3-T adsorption, especially at low OH concentrations.[29]

In addition to solvent effects, the chain length and functional groups are crucial in determining the surface composition of mixed SAMs. The constituent that has the longer chain (less soluble) has been found to experience a higher activity in solution and consequently be favored to adsorb faster.[30] For example, Liedberg have observed a close 1:1 relationship between HS-$(CH_2)_{16}$-OH and HS-$(CH_2)_{13}$-CH_3 on the surface.[22] Most of the experimental data in their study showed the points just above or below the 1:1 line and ethanol solvent was found to create a highly favored hydroxyl terminated adsorption. Since the two monolayers used in this study have the same chain length, this factor is negligible and preferential adsorption is associated with the solvent and functional groups.

3.5 Scanning Tunneling Microscopy

STM images were obtained using a Digital Instruments Nanoscope III MultiMode microscope with an atomic "A" scanner (*Note: STM images were taken at the University of South Carolina*). The tip was composed of 80 % Pt/ 20% Ir and possesses a thickness of .25 mm. The tip was cut at a 30° angle to provide an atomically sharp end. The initial parameters for each measurement were set as the following: 500 nm scan size, integral and proportional gain at 6.00 V, and a scan rate of 5.09 Hz. These parameters were adjusted accordingly to the image quality during scans. All images were acquired by applying a 1 V bias across the tip and an average tunneling current of 30 pA was observed between the tip/surface. The Au(111)/mica surface samples were used for STM measurements under ambient atmosphere conditions. In the case of the hydrophilic surface, a stream of ultra-pure N_2 was used to discard any contaminates or water vapors that were on the surface.

3.5.1 STM Results and Discussion

Scanning tunneling microscopy is a useful technique in the surface science field. The capability to view atoms by producing a "real space" image helps the qualitative analysis of SAMs on gold. Figure 3.7 shows the image of CH_3-T SAM on Au(111). The topographical feature of this particular area displays a large Au terrace. Another distinguishable observation is the "hole"-like features on the Au structure (pointed out by black arrows).

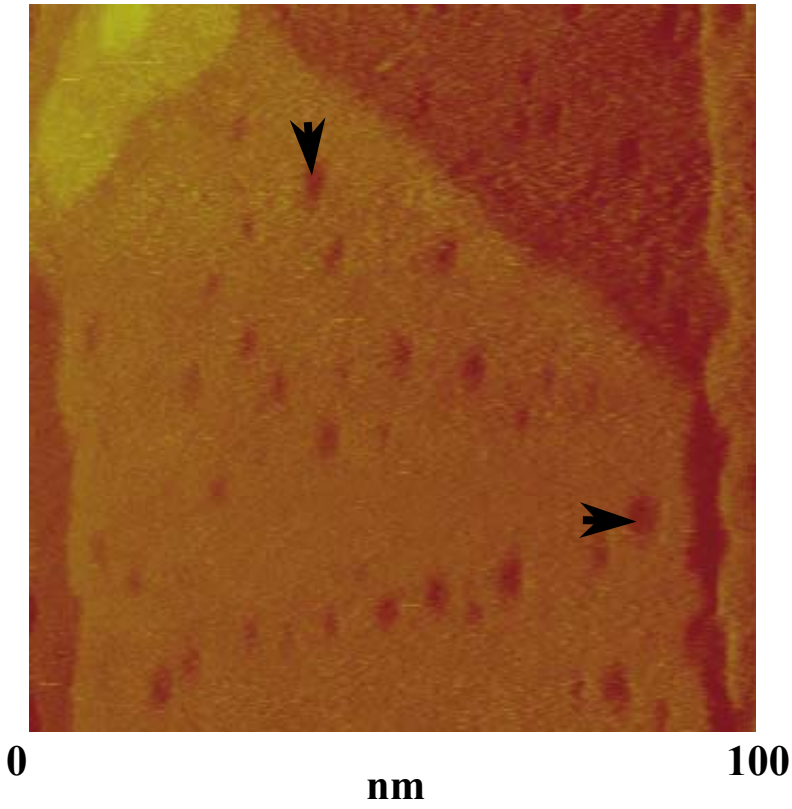

Figure 3.7. STM image of 1-dodecanethiol (CH_3-T) SAM on Au(111). Image capturing conditions: scan size (100 nm × 100 nm), tunneling current (30.5 pA), bias (1.09 V), scan rate (6.78 Hz), and z-range (10.7 nm). The black arrows show pits.

These "holes" or "pits" are actually depressions in the Au surface layer originating from an etching process during the adsorption of SAMs.[32] The depression depths are usually on the order of 2.5 Å and this is in agreement with the Au(111) single-atom step height.[33] Missing Au surface atoms caused by etching has been verified through the detection of dissolved Au in the ethanolic solutions from which the SAMs are prepared.[32,33] Other studies[20,34] have confirmed this phenomenon and provided much more insight on the mechanism. According to Porter *et al.*,[34] the depressions are produced mainly from a reconstruction mechanism of the gold atoms, and the etching is a secondary process. In further details, the underlying Au atoms are compacted together from the adsorbate interactions with the Au substrate; as a result, voids are formed on the topmost layer. The voids are then conveyed to the domain boundaries; consequently, causing depressions in the process. The size of the depressions can vary in diameter (~2-5 nm) and the diameter of these depressions can be manipulated by an STM tip. Previous investigations have shown that the tip could move the depressions and smaller depressions would aggregate to form larger ones.[35] This can occur if the same sample area is frequently scanned.

The packing arrangement of CH_3-T SAM on Au(111) is a $(\sqrt{3} \times \sqrt{3})R30°$, where the symmetry of sulfur atoms has a hexagonal pattern with an S…S spacing of 4.97 Å and calculated area per molecule of (21.4 $Å^2$).[13,36,37] The 30° represents the angle at which the overlayer unit cell is rotated with respect to the Au substrate. The Au substrate has a $c(4 \times 2)$ superlattice unit cell (*c* stands for centered) and the sulfur atoms in the SAM are occupied at 3-fold hollow sites.[13,36-38] *This packing arrangement is modeled in Chapter 4*.

The methyl-terminated monolayers have been examined extensively because of their ease in obtaining STM images in ambient atmosphere. In contrast, the hydroxyl-terminated monolayers are lacking in this particular area of characterization due to the hydrophilic nature of the OH groups. Nevertheless, studies are still performed on these OH-T SAM and one of the most interesting features is the packing arrangement. Since the two monolayers have identical chain lengths and similar properties, the functional

groups are the only influential factor that could cause a difference in packing. Figure 3.8 depicts the image of 11-mercapto-1-undecanol on Au(111). Clearly, atomic resolution of the OH-T SAM is achievable. In Figure 3.8, the bright looking dots are the hydroxyl-terminated SAM. The overlayer structure of the OH-T monolayers is slightly different from the CH_3-T arrangement. One good explanation of this observation is the highly directional, short distance (2.6-3.0 Å) hydrogen bonding effects.[23] Since the average distance between neighboring OH groups is ~5 Å, the alkanethiols have to compensate by bending toward each other. These accommodations have a major bearing on the overlayer structure and the structure has been defined as an oblique unit cell using the mercaptohexanol model.[20] Despite their slight difference in overlayer structure, the methyl- and hydroxyl-terminated SAMs still maintain the same packing density of 21.4 $Å^2$ -per-thiolate.[39] Furthermore, the defect densities cannot be distinguished from the two types of SAMs, but it should be noted that the OH-T SAM do produce the same defect depressions as the CH_3-T SAM. Figure 3.9 illustrates the depressions along with dark lines. These lines are boundaries that delimit domains of thiol molecules. The lines are a function of solvent, temperature, and residence time of substrates in solution.[40]

The single component self-assembled monolayers show their many similarities in structure, an important feature for extending our work to mixed systems. Many arguments on whether or not the monolayers are uniformly distributed or form discrete islands on the surface are still active. Whitesides *et al*. have shown that binary mixtures containing $\{HS(CH_2)_{10}CH_3$ & $HS(CH_2)_{10}CH_2OH\}$ do not form meaningful size islands through XPS and wettability experiments.[21,29,30] Figure 3.10 shows the 50:50 mixture (solution concentration) of $\{HS(CH_2)_{11}OH$:$HS(CH_2)_{11}CH_3\}$ adsorbed on Au(111). It is extremely difficult to differentiate between OH groups and CH_3 groups in an STM image. The relative "brightness" of the two functional groups with respect to the alkyl groups is equal.[41]

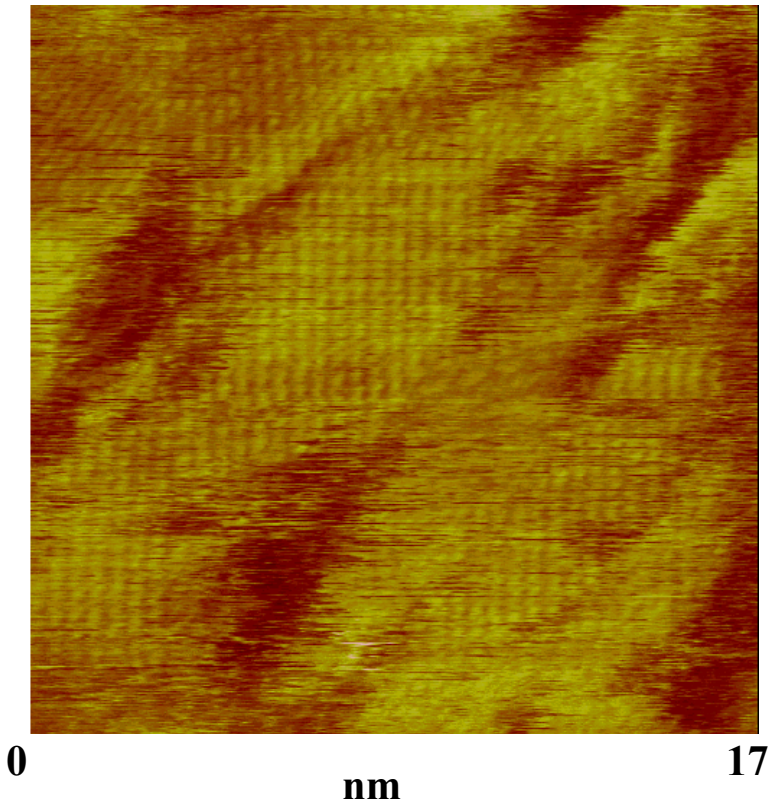

Figure 3.8. STM atomic image of 11-mercapto-1-undecanol (OH-T) on Au(111). Image capturing conditions: scan size (17.2 nm × 17.2 nm), tunneling current (30.5 pA), bias (1 V), scan rate (12.21 Hz), and z-range (2.00 nm). Bright looking spots are OH-T SAM (*Note: horizontal streaking in the image is caused by background noise)*.

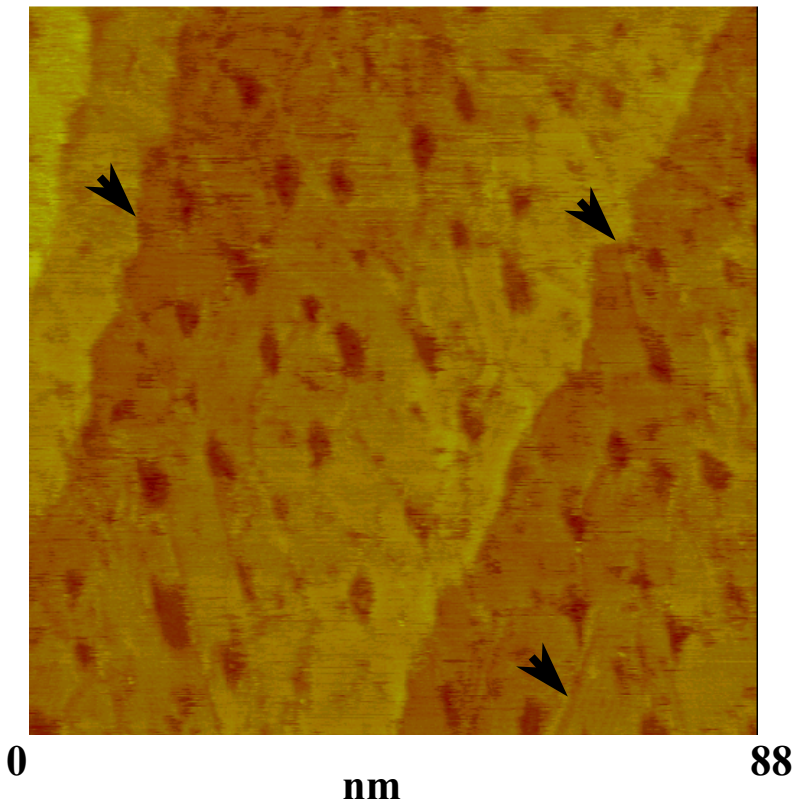

Figure 3.9. STM image of 11-mercapto-1-undecanol (OH-T) on Au(111). Image capturing conditions: scan size (87.7 nm × 87.7 nm), tunneling current (30.5 pA), bias (1 V), scan rate (10.17 Hz), and z-range (5.00 nm). Black arrows show depressed lines.

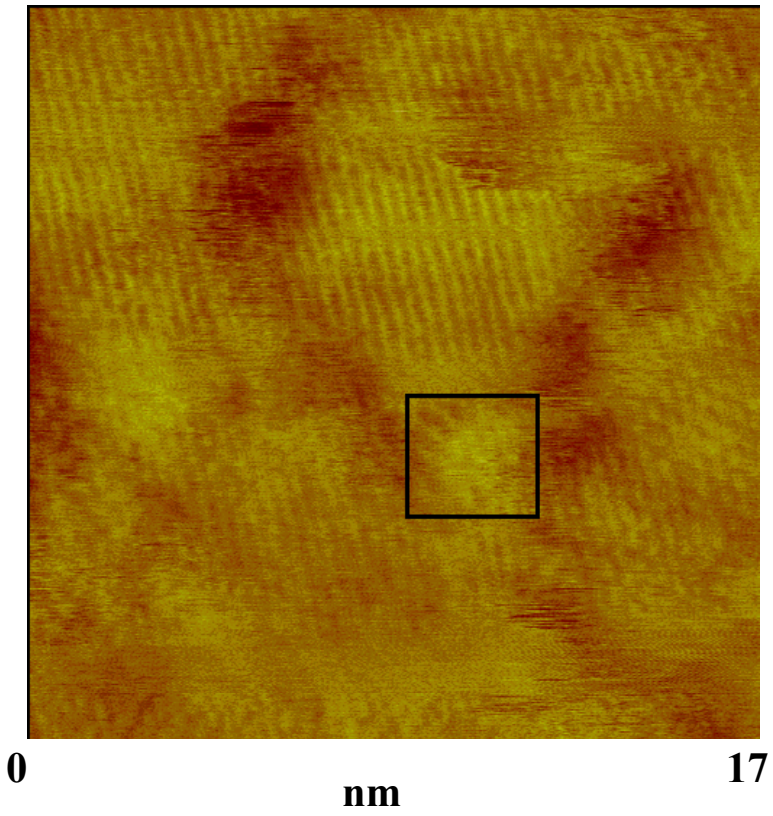

Figure 3.10. STM atomic image of 50 % 11-mercapto-1-undecanol & 50 % 1-dodecanethiol on Au(111). Image capturing conditions: scan size (17 nm × 17 nm), tunneling current (36.9 pA), bias (1 V), scan rate (30.52 Hz), and z-range (3.00 nm). The black box might indicate OH-T aggregation.

3.6 Temperature-Programmed Desorption

TPD measurements performed in the UHV main chamber used an Omega® CN3000 microprocessor dual input controller and Kepco power supply. Gold substrates were mounted onto the copper block inside the chamber and a thermocouple wire monitored the surface temperature. The base pressure inside the main chamber operated on the order of 10^{-10} mbar. The manipulator was rotated to 188°, which aligned the surface normal directly to the QMS detector. A heater inside the Cu block provided the source to heat the surfaces by applying 4 V and 4 amps via electrical feedthroughs. The mass signal intensities were recorded using the multichannel scaler.

3.6.1 TPD Results and Discussion

Temperature-programmed desorption provides important information about the gold-thiolate bond energy and intermolecular interactions of alkyl groups.[42] Figure 3.11 shows $S(CH_2)_{11}CH_3$ molecules desorbing from a pure CH_3-T SAM covered Au(111) substrate. A previous study by Nuzzo *et al.*[43] concluded that the monolayers associatively desorb as disulfides at 450-500 K; however, Poirier[44] have shown that butanethiol molecules on Au(100) desorb as thiols. Figure 3.11 clearly shows that the molecules desorbing are disulfides (Figure 3.12) and not individual thiol molecules (*parent mass of* $\{CH_3(CH_2)_{11}SS(CH_2)_{11}CH_3\}$ *is 402 amu*). The major intense peak occurring at 425 K indicates the high-density phase of disulfides desorbing and the peak tailing is a result of second-order desorption. The TPD experiment indicates that there is only a single monolayer on the surface and not a multi-layer. For instance, Nishida[45] observed two desorption peaks at ~330 K and 490 K for octadecanethiol on Au(111). The peak at 330 K is a characteristic of physisorption molecules, which can arise from lack of rinsing the surface thoroughly.

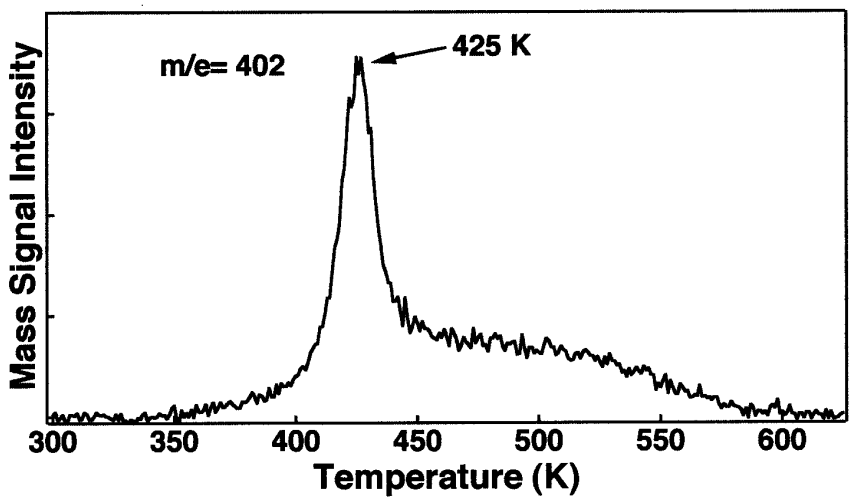

Figure 3.11. TPD spectrum of $\{CH_3(CH_2)_{11}SS(CH_2)_{11}CH_3\}$ with a parent mass of 402 amu. The highly intense peak indicates desorbing chemisorb species and the peak tailing is a result of second-order desorption.

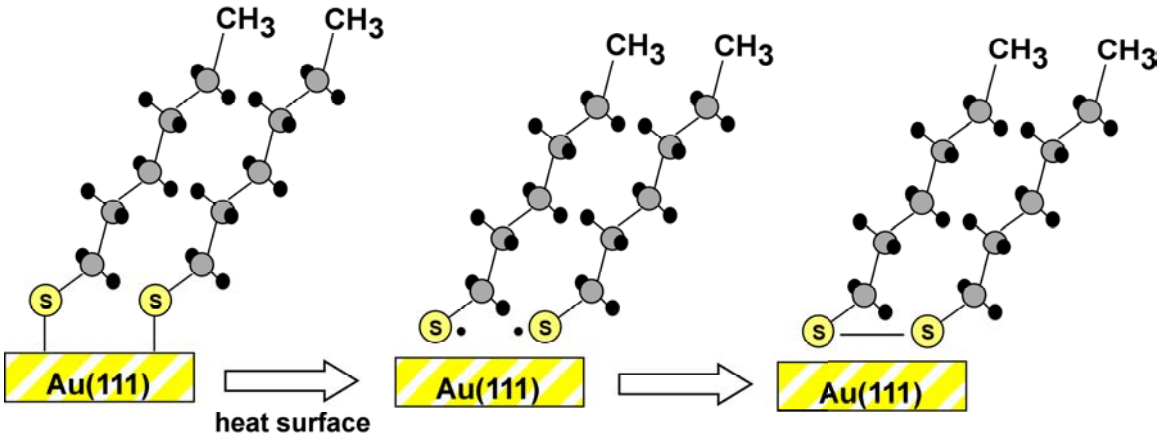

Figure 3.12. Shows the mechanism of forming disulfides. Radical thiolates are formed and the molecules desorb as disulfides. The homolytic bond strength of the Au-S bond has been estimated to be 44-45 kcal/mol and the S-S bond is ~60 kcal/mol.[46]

3.7 Summary

SAMs make good model surfaces because they are well-defined, stable, and most importantly, their terminal groups provide the opportunity to examine how gas-surface energy transfer depends on surface structure and chemical functionality. 11-Mercapto-1-undecanol (OH-terminated) and 1-dodecanethiol (CH_3-terminated) are used to create these model surfaces. SAMs are chemisorbed on Au(111) substrates by immersing them in the proper alkythiol/ethanolic solution and two types of substrates are used, glass posterior and mica posterior substrates. These molecular assemblies are characterized by XPS, STM, TPD, and RAIRS. XPS results showed preferential adsorption of CH_3-T molecules and STM images illustrated the defect depressions that originate from the adsorption process. TPD measurements confirmed that only one layer of thiolates is present on the surface.

Chapter 4

Results and Analysis: Argon Scattering

4.1 High-E_i Ar Scattering

Gas-surface energy transfer experiments are accomplished by directing a nearly monoenergetic Ar atomic beam at a surface composed of OH-terminated (OH-T) or CH_3-terminated (CH_3-T) SAMs on gold. The peak incident energy for the high-energy beam in this study is 80 kJ/mol (13 kJ/mol full width at half maximum). The flight times of the Ar atoms are obtained as they travel from a rotating chopper wheel, scatter away from the surface, and pass through an aperture into a quadrupole mass spectrometer. The raw mass spectrometer signal is proportional to the number density N(t), and is used to compute the probability, $P(E_f)$, that an Ar atom leaves the surface with final energy, E_f. The translational energy distributions are computed from the relations $E_f = (1/2)m_{Ar}(L/t)^2$ and $P(E_f) \sim t^2N(t)$, where t is the Ar atom flight time and L is the distance between the surface and the ionizer of the mass spectrometer.[47] All spectra are rectified for electronic and timing offsets and the flight time from the chopper wheel to the surface is subtracted from each spectrum.

Figure 4.1 shows the time-of-flight (TOF) data for Ar atoms scattering from clean Au(111), pure OH-T, and pure CH_3-T surfaces. The high velocity peak at early arrival times (~300 μs) is evident of inelastic scattering (IS), where the atoms undergo a single collision event and maintain most of their incident energy. The broad component at later arrival times indicates the atoms that have lost the majority of their excess energy due to thermalization on the surface before desorbing with a Boltzmann velocity distribution. These two particular scattering channels are more apparent in the corresponding energy distributions. The energy distributions are separated into IS and thermal-desorption (TD) by assigning the TD channel to the component of $P(E_f)$ that falls within a Boltzmann

distribution[6]: $P_{TD}(E_f) = E_f(RT_{surf})^{-2} \exp(-E_f/RT_{surf})$. The IS contribution is assigned to the difference between $P(E_f)$ and $P_{TD}(E_f)$. The dynamics of gas-surface collisions are revealed through analysis of the fractional energy transferred to the surface in the IS channel, $(E_i - \langle E_{IS} \rangle)/E_i$, and the fraction of atoms that recoil (at the 30° specular angle) with a thermal distribution of velocities (TD fraction). The TD fraction is defined as the weighting coefficient, α in the relation: $P(E_f) = \alpha P_{TD}(E_f) + (1-\alpha)P_{IS}(E_f)$.[48]

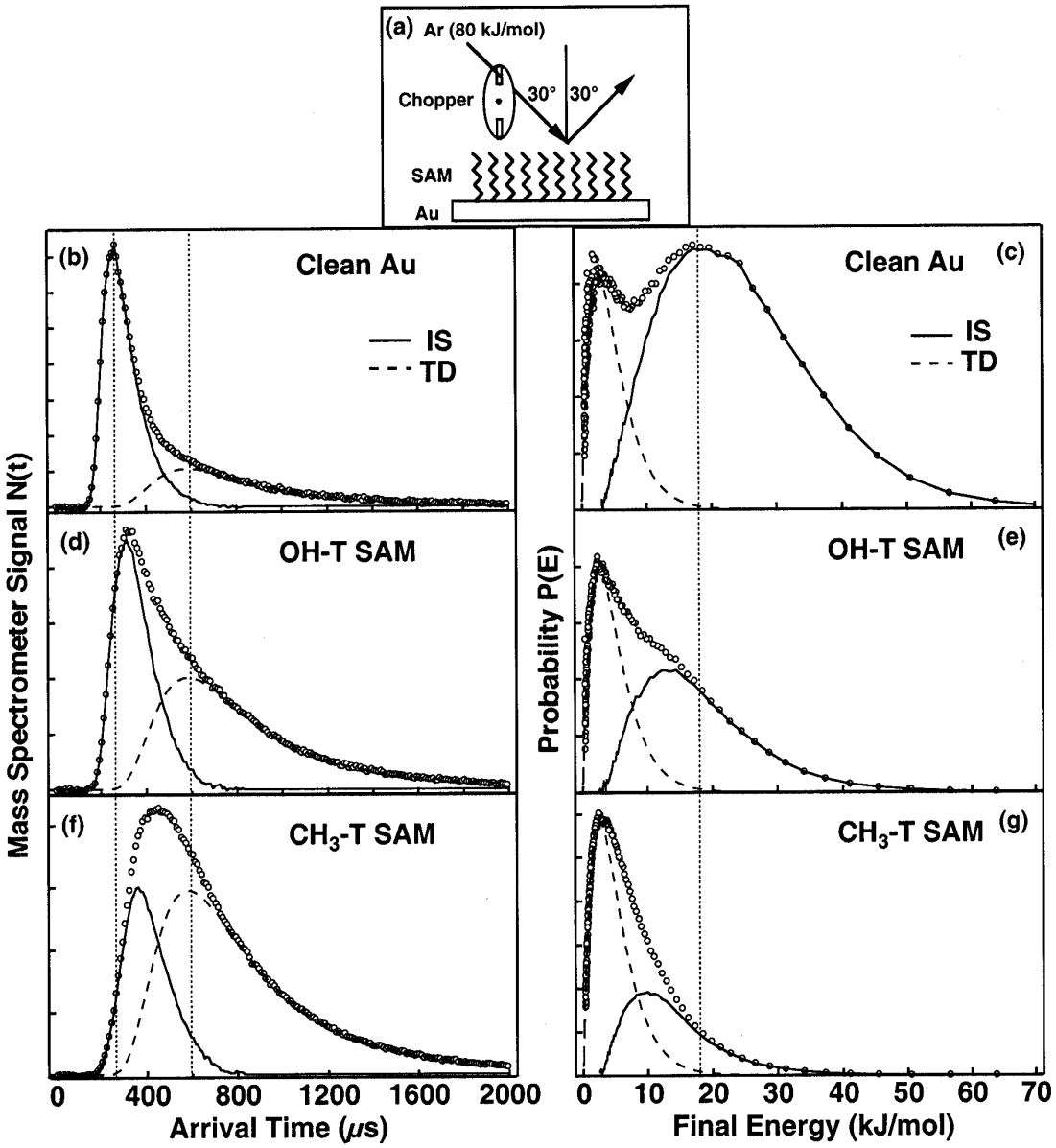

Figure 4.1. (a) Experimental geometry. (b), (d), and (f) show the time-of-flight spectra for high incident energy (80 kJ/mol) Ar scattering from a clean bare Au(111) surface, an OH-T SAM, and a CH_3-T SAM on Au, respectively. (c), (e), and (g) show the corresponding translational energy distributions for Ar scattering from a clean bare Au(111) surface, an OH-T SAM, and a CH_3-T SAM on Au, respectively. The data in each frame are normalized to a common peak value. The dashed curve is a Boltzmann distribution at the temperature of the surface, and the solid lines are the calculated inelastic scattering components. The vertical dotted lines are used to guide the eye.

The fractional energy transferred to the clean gold surface is $\langle \Delta E_{IS} \rangle / E_i = 0.69 \pm .01$, while it is greater than 0.77 for the monolayer-covered surfaces. This result is in agreement with the work of Hanley and co-workers in which they found that high-energy ion scattering from clean Au(111) is significantly more elastic than scattering from a $HS(CH_2)_5CH_3$ self-assembled monolayer on Au.[49,50] In addition, Ar atoms tend to reach thermal equilibrium much more readily on the monolayer-covered surfaces. The fraction of molecules that recoil from the surface with a Boltzmann-like energy distribution is only $0.22 \pm .01$ for bare Au, and it is a factor of two greater for the OH-T SAM and almost three times greater for the CH_3-T SAM.

The differences between scattering from the clean gold surface and the SAMs are not unexpected and can likely be attributed to a combination of factors. The monolayer-covered surface should provide several additional degrees-of-freedom into which the translational energy of the atom can be partitioned. Furthermore, kinematic arguments predict that energy transfer increases as the mass of the surface decreases.[8,9,51] It would take approximately 13 methyl groups, each with a mass of 15 amu, to equal the mass of one Au atom (197 amu). As shown in Figure 4.2, an impinging Ar atom likely interacts with at most three methyl groups on the initial collision. Therefore, it is likely that the effective mass of the monolayer-covered surface is much lower than that of the bare gold surface, which should facilitate energy transfer. Finally, the SAMs may present a more corrugated surface than clean gold. Greater corrugation, the result of either the actual surface structure or penetration of the atoms into the monolayer, is expected to lead to multiple collisions and greater energy transfer.[7]

In the studies presented here, the CH_3-T surface has additional or slightly different energy modes, relative to the OH-T surface, into which the kinetic energy of the impinging particle can be partitioned (see Table 4.1). The CH_3 torsional mode (~2 kJ/mol), as well as the stretching (~37 kJ/mol) and deformation modes (~15 kJ/mol), are well within the energy range of the impinging Ar atoms (80 kJ/mol). Impulsively scattered Ar looses, on average, 4.3 kJ/mol more energy to the CH_3-T surface than to the OH-T surface. More efficient coupling of the incident energy into the R-CH_3 torsional

mode, than into the R-OH torsional mode (~6 kJ/mol), may help explain the observed energy differences for the scattered atoms.

Table 4.1. Available energy modes for terminal groups and Ar incident energies.

Modes	**Energies**
CH_3 Stretching	37 kJ/mol
CH_3 Deformation	15 kJ/mol
CH_3 Torsion	2 kJ/mol
OH Stretching	38 kJ/mol
R-OH Torsion	6 kJ/mol
OH---O Bonding	20 kJ/mol
High-E_i Ar	80 kJ/mol
Low-E_i Ar	40 kJ/mol

Although these intuitive arguments help explain the differences in scattering from the clean bare gold and the monolayer-covered surfaces, it is not immediately clear why the OH-T and the CH_3-T surfaces lead to significantly different scattering dynamics. The TD fraction is a factor of 1.5 greater for the CH_3-T SAM and the fractional energy transfer in the IS channel is also significantly larger. The data also shows that over 83 % of the incident energy is transferred to the CH_3-T surface, while 77 % of the energy is transferred to the OH-T surface. These results are indicative of differences in the roughness and/or the rigidity of the OH-T SAM relative to the CH_3-T SAM. To fully resolve these issues, we turn to previous atomic beam experiments aimed specifically at probing the effect of surface roughness on scattering.

Nathanson *et al*. have performed atomic beam experiments to explore the surface corrugation of liquid perfluorinated polyether.[52] In this work, they investigated the effect of temperature on the scattering dynamics. Simulations of the liquid structure revealed a significant change in surface corrugation over an 85 K temperature range. Despite the large temperature-induced corrugation, they observed virtually no change in the IS energy distributions for 93 kJ/mol Ar atoms scattering from this surface over a wide

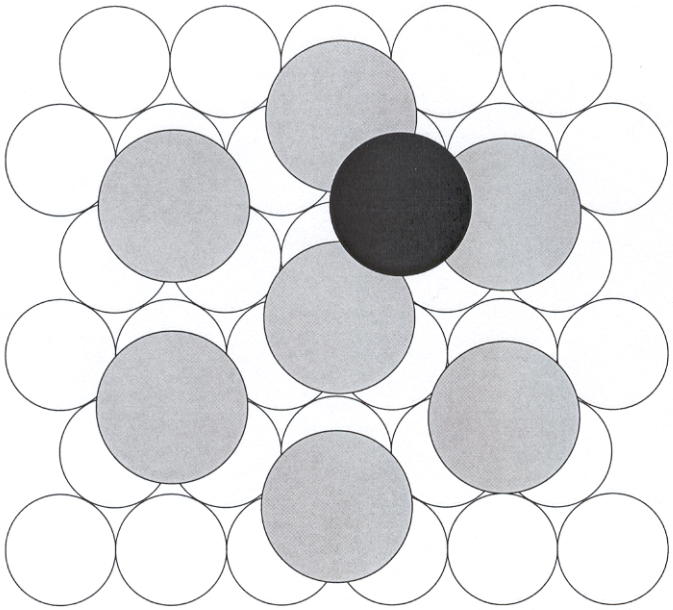

Figure 4.2. Shows the schematic unit cell for a methyl-terminated self-assembled monolayer on Au(111). The packing arrangement for CH_3-T SAM on Au(111) is represented by $(\sqrt{3} \times \sqrt{3})R30°$ hexagonal based lattice. Open circles depict the gold lattice, gray circles represent the methyl groups, and the black circle represents the van der Waals radius of an Ar atom.

temperature range of 278 to 363 K. In addition, the energy distribution of the IS component did not broaden significantly. These results, along with angle-resolved studies,[53] suggest that the inelastic channel for in-plane scattering is dominated by single hard-sphere-like collision events, even on highly corrugated surfaces.

Figure 4.3 is a direct comparison of energy distributions of the IS channel for Ar scattering from the OH-T and CH_3-T surfaces. The peak and the mean of the energy distribution for the CH_3-T surface shift to lower energies relative to the OH-T surface. In addition, there is a significant narrowing of the CH_3-T $P_{IS}(E)$ distribution.

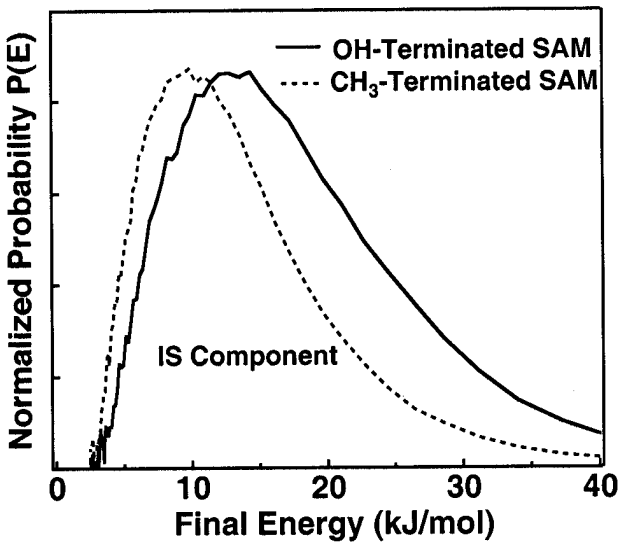

Figure 4.3. Comparison of the IS components of the $P(E_f)$ distributions for 80 kJ/mol Ar scattering from OH-T (solid line) and CH_3-T (dashed line) SAMs. The peak values of the distributions are normalized.

This comparison indicates that any subtle differences in the roughness of the CH_3-T and OH-T systems are not responsible for the observed scattering dynamics. Rather, it appears that the OH-T monolayer is more rigid, i.e., it has a higher effective surface mass than the CH_3-T SAM. The relatively high effective mass of the OH-T system may originate from physical characteristics, such as the molecular weight of the hydroxyl compared to methyl terminal groups or from hydrogen-bonding within the OH-T monolayer that may add structural rigidity to the surface.

Insight into the effective mass of the surface is obtained through analysis of the fractional energy transfer of impulsively scattered atoms. Many studies have used a "hard-cube" approximation equation to model the types of collisions that lead to impulsive scattering.[51] The equation predicts that as the surface mass increases, the fractional energy transferred to the surface decreases.

Table 4.2. Summary of results for 80 kJ/mol Ar scattering from clean Au and SAMs.

Surface	**TD fraction**	**Energy Transfer E_i - $\langle E_{IS} \rangle / E_i$**	**$P_{IS}(E)$ width (FWHM)**
Clean Au	0.22 ± .01	0.69 ± .02	27.4 ± 1 kJ/mol
Au-S$(CH_2)_{11}$OH	0.42 ± .01	0.77 ± .02	18.4 ± 1 kJ/mol
Au-S$(CH_2)_{11}CH_3$	0.60 ± .01	0.83 ± .02	13.5 ± 1 kJ/mol

In order to validate whether the heavier OH groups alone account for the observed scattering dynamics, scattering argon from an OD-terminated SAM is employed. Submersing the OH-T SAM in D_2O for 1 hr can create this surface. Temperature-programmed desorption is used to characterize the OD-terminated SAM. Figure 4.4 shows a comparison between Ar scattering from the two surfaces, and the spectra are virtually indistinguishable. Since a change in the mass of the outer most functional group by 1 amu has a negligible effect on the scattering dynamics, the higher effective mass of the OH-T monolayer relative to the CH_3-T monolayer is likely not due to the 2 amu mass difference between the two terminal groups.

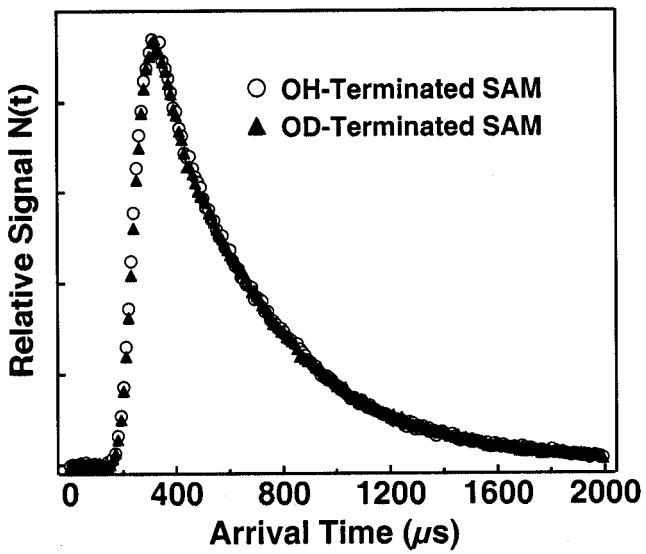

Figure 4.4. Comparison of 80 kJ/mol Ar scattering from OH-T and OD-T SAMs. The nearly identical spectra indicate that the difference in surface mass of 1 amu has a negligible effect on the scattering dynamics.

4.2 Low-E_i Ar Scattering

In collisions of high-incident-energy Ar atoms with gold, the fractional energy transfer and the extent of thermalization are significantly enhanced when the surface is covered with a self-assembled monolayer composed of CH_3-T molecules. This increase in energy transfer may be due to more penetration below the chain terminal groups for the CH_3-T than for the OH-T SAM. To test this hypothesis, a low incident energy Ar beam is employed to reduce the potential for ballistic penetration into the monolayers. According to Hase, penetration into the monolayer plays a much less significant role in the energy transfer dynamics for lower-incident-energy atoms.[7] Figure 4.5 shows the TOF data for 40 kJ/mol Ar scattering from the pure OH-T and pure CH_3-T SAMs. The peaks are broad; single peaked, and shifted to longer arrival times than the corresponding

high-energy spectra. In addition, the data shows much greater propensity for thermalization for the lower energy Ar atoms; however, the trend in the extent of energy transfer for the two surfaces is remarkably similar to that for the high-energy beams. This is not surprising since the monolayer-covered surfaces are closely packed. Although surface penetration may participate in the overall scattering dynamics, it seems unlikely that differences in the extent of penetration for the two monolayers are responsible for the observed trends.

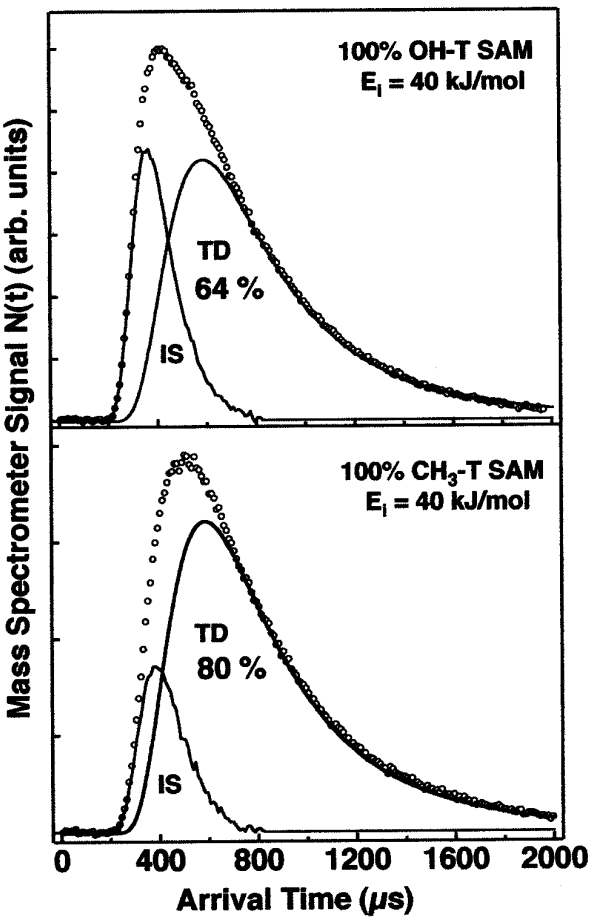

Figure 4.5. Comparison of 40 kJ/mol Ar scattering from OH-T and CH_3-T SAMs. 64 % of the atoms undergo thermal-desorption for the pure OH-T and 80 % of the atoms undergo thermal-desorption for the pure CH_3-T.

It appears that subtle differences in the physical characteristics of the two systems do not account for the observed trends in energy transfer and thermal-desorption fractions. Therefore, the chemical nature of the OH-T SAM must play a major role in determining the outcome of the gas-surface collision. Previous studies using reflection-absorption infrared spectroscopy have revealed that the terminal OH groups of an alkanethiol SAM form a hydrogen-bonding network across the surface.[22,54] This network anchors the end groups of the alkane chains thereby rendering the individual surface molecules less flexible than the monolayer composed of CH_3-T alkanethiols.

4.3 Ar Scattering from Mixed Monolayers

Scattering from an OH-T surface vs. CH_3-T has provided a significant to the scattering dynamics and energy transfer; however, the effects of hydrogen bonding on scattering are still not fully understood. To consider the chemical nature of the OH-T SAM, studies of Ar (80 kJ/mol) scattering on surfaces composed of mixed SAMs containing OH- and CH_3-terminated alkanethiols are performed. Eleven surfaces ranging in OH concentrations from 100 % to 0 % have been studied. Figure 4.6 shows TOF distributions for scattering from the mixed monolayers at five representative surface compositions. These spectra show a change in the intensity of the impulsively scattered channel (sharp peak at early times) relative to the broad thermal component as the surface OH concentration decreases from 100 % to 30 %. However, there is a remarkably small change in the TOF distributions as the OH concentration decreases further to the pure CH_3-T surface. Two important observations emerge from this comparison: (1) the decrease in the IS component with decreasing OH concentration is accompanied by an increase in the intensity of the TD component and (2) the TOF spectra for all OH concentrations below 30 % are identical to within the signal-to-noise level.

Another important observation that needs to be considered is the surface rigidity in mixed SAMs. As mentioned in the previous section, the TOF distributions do not change significantly below 30 % [OH]. The extent of energy transfer and thermalization increases as the amount of interfacial hydrogen bonding decreases to the point where it is

insignificant. In Figure 4.6, it appears that the interfacial hydrogen bonding is disrupted sufficiently enough that the majority of the OH-T alkanethiols on the surface behave as independent alkane chains able to adsorb energy into every available mode. This observation is more evident in Figure 4.7. The TD fraction and fractional energy transfer increases as the OH concentration decreases until the OH surface concentration reaches ~30 %. At this point, the fractional energy transfer is no longer increasing with respect to decreasing OH surface concentration.

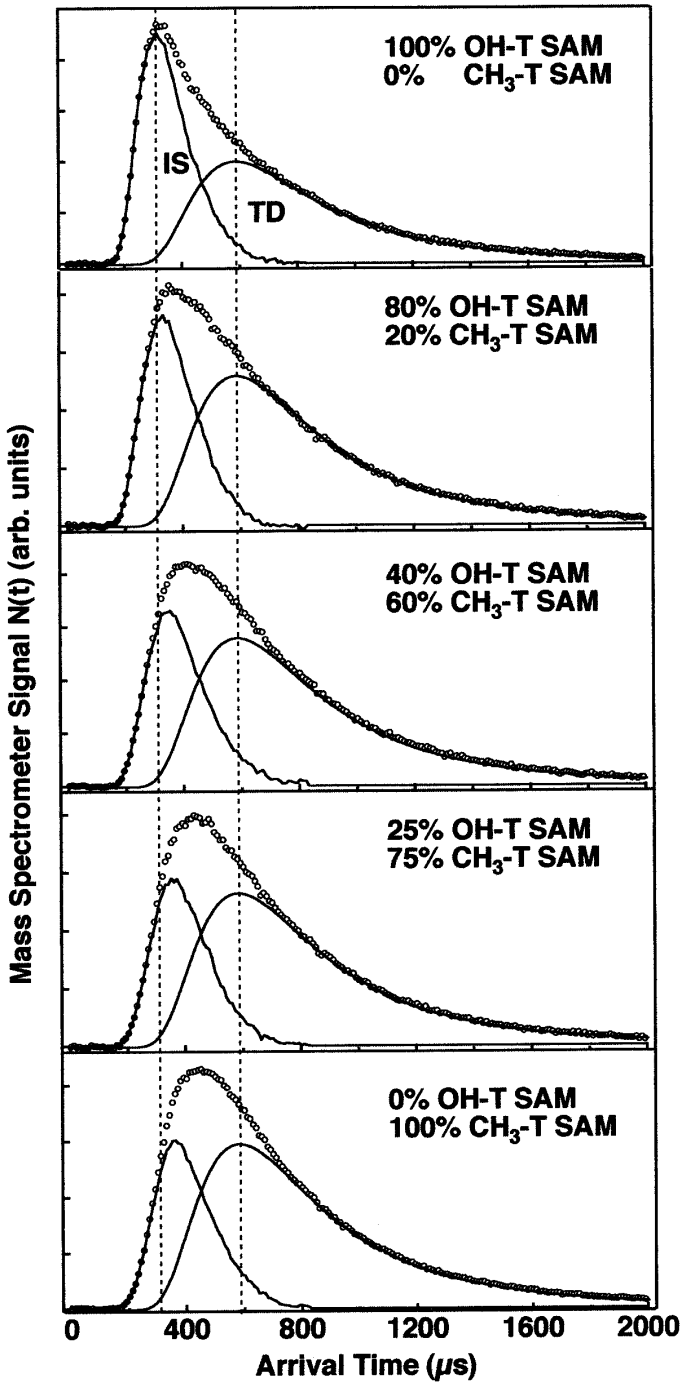

Figure 4.6. Comparison of Ar (80 kJ/mol) scattering from different OH surface concentrations. The dashed lines are used to guide the eye.

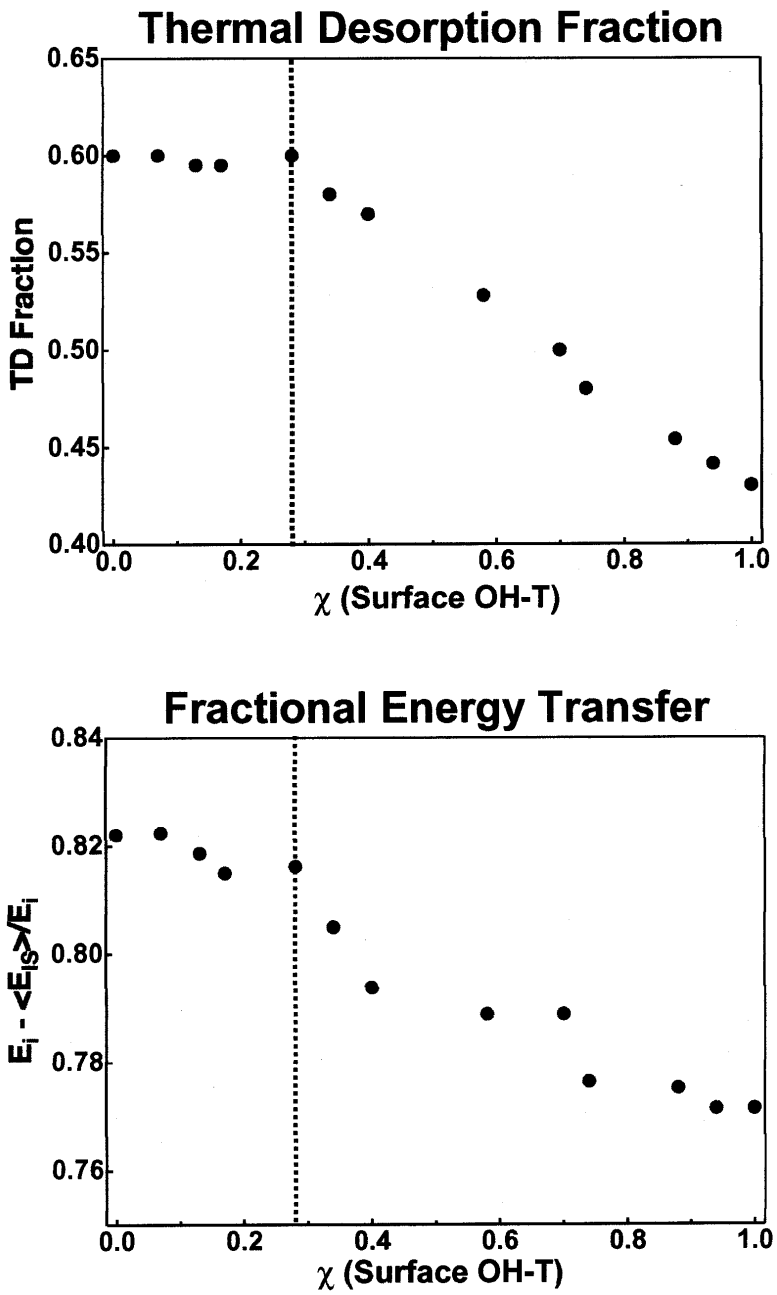

Figure 4.7. Comparison of TD fraction and fractional energy transfer with respect to mole fraction of OH assembly on the surface. The dashed lines are used to guide the eye.

4.4 Summary

Gas-surface energy transfer experiments are accomplished by directing an Ar atomic beam at a clean Au(111) surface and surfaces composed of OH-terminated or CH_3-terminated SAMs on Au(111). The fractional energy transferred to the clean gold surface is 69 %, while it is greater than 77 % for the monolayer-covered surfaces. The extent of thermalization on the surface during the collision is significantly greater for the CH_3-T surface than for the OH-T surface. The thermal-desorption fraction is a factor of ~1.5 greater for the CH_3-T surface. Since the two monolayers are similar in structure, packing density, and mass, the differences in scattering dynamics are likely due to a combination of factors that may include differences in the available energy modes between the two terminal groups and the hydrogen-bonding nature of the OH-T SAM. The time-of-flight distributions of mixed SAMs support this hypothesis and shown that as the OH surface concentration decreases, the fractional energy transferred and thermal-desorption fraction increases.

References

(1) Klassen, J. K.; Fiehrer, K. M.; Nathanson, G. M. *J. Phys. Chem. B* **1997**, *101*, 9098.
(2) Morris, J. R.; Behr, P.; Antman, M .D.; Ringeisen, B. R.; Splan, J.; Nathanson, G. M. *J. Phys. Chem. A* **2000**, *104*, 6738.
(3) Behr, P.; Morris, J. R.; Antman, M. D.; Ringeisen, B. R.; Splan, J. R.; Nathanson, G. M. *Geophys. Res. Lett.* **2001**, *28*, 1961.
(4) Ceyer, S. T. *Science* **1990**, *249*, 133.
(5) Hurst, J. E.; Becker, C. A.; Cowin, J. P.; Janda, K. C.; Wharton, L.; Auerbach, D. J. *Phys. Rev. Lett.* **1979**, *43*, 1175.
(6) Yan, T.; Hase, W. L.; Barker, J. R. *Chem. Phys. Lett.* **2000**, *329*, 84.
(7) Yan, T.; Hase, W. L. *Phys. Chem. Chem. Phys.* **2000**, *4*, 901
(8) Paz, Y.; Naaman, R. *J. Chem. Phys.* **1991**, *94*, 4921.
(9) Cohen, S. R.; Naaman, R.; Sagiv, J. *Phys. Rev. Lett.* **1987**, *58*, 1208.
(10) Rettner, C. T.; Auerbach, D. J.; Tully, J. C.; Kleyn, A. W. *J. Phys. Chem.* **1996**, *100*, 13021.
(11) Klassen, J. K.; Nathanson, G. M. *Science* **1996**, *273*, 333.
(12) Nathanson, G. M.; Davidovits, P.; Worsnop, D. R.; Kolb, C. E. *J. Phys. Chem.* **1996**, *100*, 13007.
(13) Ulman, A. *Chem. Rev.* **1996**, *96*, 1533.
(14) McCash, E. M. *Surface Chemistry*, Oxford; (New York: Oxford University Press, **2001**).
(15) Rossiter, B. W.; Hamilton, J. F.; Baetzold, R. C. *Physical Methods of Chemistry*, 2nd ed., (New York: Wiley, **1988**).
(16) Ulman, A. *Introduction to Ultrathin Organic Films*, (Academic Press: Boston, **1991**).
(17) Sabapathy, R. C.; Crooks, R. M. *Langmuir* **2000**, *16*, 1777.
(18) Bain, C. D.; Troughton, E. B.; Tao, Y.; Evall, J.; Whitesides, G. M.; Nuzzo, R. G. *J. Am. Chem. Soc.* **1989**, *111*, 321.
(19) Delamarche, E.; Michel, B.; Kang, H.; Gerber, Ch. *Langmuir* **1994**, *10*, 4103.
(20) Poirier, G. E. *Chem. Rev.* **1997**, *97*, 1117.
(21) Bain, C. D.; Biebuyck, H. A.; Whitesides, G. M. *Langmuir* **1989**, *2*, 723.
(22) Bertilsson, L.; Liedberg, B. *Langmuir* **1993**, *9*, 141.
(23) Sprik, M.; Delamarche, E.; Michel, B.; Röthlisberger, U.; Klein, M. L.; Wolf, H.; Ringsdorf, H. *Langmuir* **1994**, *10*, 4116.
(24) Nuzzo, R. G.; Dubois, L. H.; Allara, D. L. *J. Am. Chem. Soc.* **1990**, *112*, 558.
(25) Porter, M. D.; Bright, T. B.; Allara, D. L.; Chidsey, C. E. D. *J. Am. Chem. Soc.* **1987**, *109*, 3359.
(26) Dunbar, T. D.; Cygan, M. T.; Bumm, L. A.; McCarty, G. S.; Burgin, T. P.; Reinerth, W. A.; Jones II, L.; Jackiw, J. J.; Tour, J. M.; Weiss, P. S.; Allara, D. L. *J. Phys. Chem. B* **2000**, *104*, 4880.
(27) Castner, D. G.; Hinds, D.; Grainger, D. W. *Langmuir* **1996**, *12*, 5083.
(28) Zubrägel, Ch.; Deuper, C.; Schneider, F.; Neumann, M.; Grunze, M.; Schertel,

A.; Wöll, Ch. *Chem. Phys. Lett.* **1995**, *238*, 308.
(29) Bain, C. D.; Evall, J.; Whitesides, G. M. *J. Am. Chem. Soc.* **1989**, *111*, 7155.
(30) Bain, C.D.; Whitesides, G. M. *J. Am. Chem. Soc.* **1989**, *111*, 7164.
(31) Chen, S.; Li, L.; Boozer, C. L.; Jiang, S. *J. Phys. Chem. B* **2001**, *105*, 2975.
(32) Schönenberger, C.; Sondag-Huethorst, J. A. M.; Jorritsma, J.; Fokkink, L. G. J. *Langmuir* **1994**, *10*, 611.
(33) Edinger, K.; Gölzhäuser, A.; Demota, K.; Wöll, Ch.; Grunze, M. *Langmuir* **1993**, *9*, 4.
(34) McDermott, C. A.; McDermott, M. T.; Green, J.; Porter, M. D. *J. Phys. Chem.* **1995**, *99*, 13257.
(35) Dürig, U.; Züger, O.; Michel, B.; Häussling, L.; Ringsdorf, H. *Phys. Rev. B* **1993**, *48*, 1711.
(36) Camillone III, N.; Chidsey, C. E. D.; Liu, G.; Scoles, G. *J. Chem. Phys.* **1993**, *98*, 3503.
(37) Fenter, P.; Eberhardt, A.; Eisenberger, P. *Science* **1994**, *266*, 1216.
(38) Touzov, I.; Gorman, C. B. *J. Phys. Chem. B* **1997**, *101*, 5263.
(39) Poirier, G. E.; Pylant, E. D.; White, J. M. *J. Chem. Phys.* **1996**, *104*, 7325.
(40) Delamarche, E.; Michel, B. *Thin Solid Films* **1996**, *273*, 54.
(41) Cyr, D. M.; Venkataraman, B.; Flynn, G. W.; Black, A.; Whitesides, G. M. *J. Phys. Chem.* **1996**, *100*, 13747.
(42) Lavrich, D. J.; Wetterer, S. M.; Bernasek, S. L.; Scoles, G. *J. Phys. Chem. B* **1998**, *102*, 3456.
(43) Nuzzo, R. G.; Zegarski B. R.; Dubois, L. H. *J. Am. Chem. Soc.* **1987**, *109*, 733.
(44) Poirier, G. E.; *J. Vac. Sci.* **1996**, *14*, 1453.
(45) Nishida, N.; Hara, M.; Sasabe, H.; Knoll, W. *Jpn. J. Appl. Phys.* **1996**, *35*, 5866.
(46) Kondoh, H.; Kodama, C.; Sumida, H.; Nozoye, H. *J. Chem. Phys.* **1999**, *111*, 1175.
(47) Auerbach, D. J.; Comsa, G.; Poelsema, B.; Asscher, M.; Somorjai, G. *Atomic and Molecular Beam Methods*, edited by Scoles, G. (Oxford University, New York, **1988** & **1992**), vols. I and II.
(48) Saecker, M. E.; Nathanson, G. M. *J. Chem. Phys.* **1993**, *99*, 7056.
Wainhaus, S. B.; Lim, H.; Schultz, D. G.; Hanley, L. *J. Chem. Phys.* **1997**, *106*, 10329.
(50) Schultz, D. G.; Wainhaus, S. B.; Hanley, L.; de Sainte Claire, P.; Hase, W. L. *J. Chem. Phys.* **1997**, *106*, 10337.
(51) Grimmelmann, E. K.; Tully, J. C.; Cardillo, M. J. *J. Chem. Phys.* **1980**, *72*, 1039.
(52) King, M. E.; Saecker, M. E.; Nathanson, G. M. *J. Chem. Phys.* **1994**, *101*, 2539.
(53) King, M. E.; Nathanson, G. M.; Hanning-Lee, M. A.; Minton, T. K. *Phys. Rev. Lett.* **1993**, *70*, 1026.
(54) Pan, S.; Castner, D. G.; Ratner, B. D. *Langmuir* **1998**, *14*, 354

Vita

Shelby F. Shuler was born to John and Eva Shuler on April 18, 1977 in Columbia, South Carolina. He has two older brothers, Larmarte and Damon. Shelby graduated from Keenan High School in 1995 and enrolled at The University of South Carolina in 1996. He received his Bachelor of Science degrees in Chemistry and Marine Science on December 13, 1999. After graduating, Shelby was a research assistant with Dr. Uwe H. F. Bunz in the Department of Chemistry at USC. In August 2000, he entered Virginia Tech and began research on molecular beam studies with Dr. John R. Morris to earn a Master of Science degree.